

*Sister Rod Destructive Examinations (FY21)*

# ***Appendix C: Rod Internal Pressure, Void Volume, and Gas Transmission Tests***

## **Spent Fuel and Waste Disposition**

*Prepared for  
US Department of Energy  
Spent Fuel and Waste Science  
and Technology*

*Oak Ridge National Laboratory  
Robert N. Morris,  
Rose Montgomery, and  
Paul Cantonwine*

***March 31, 2022***

**M2SF-22OR010201042**

**ORNL/SPR-2021/2278**

**ORNL/SPR-2020/1769 Revision 1**

This report was prepared as an account of work sponsored by an agency of the United States Government. Neither the United States Government nor any agency thereof, nor any of their employees, makes any warranty, express or implied, or assumes any legal liability or responsibility for the accuracy, completeness, or usefulness of any information, apparatus, product, or process disclosed, or represents that its use would not infringe privately owned rights. Reference herein to any specific commercial product, process, or service by trade name, trademark, manufacturer, or otherwise, does not necessarily constitute or imply its endorsement, recommendation, or favoring by the United States Government or any agency thereof. The views and opinions of authors expressed herein do not necessarily state or reflect those of the United States Government or any agency thereof.

## SUMMARY

This report documents work performed under the Spent Fuel and Waste Disposition's Spent Fuel and Waste Science and Technology program for the US Department of Energy (DOE) Office of Nuclear Energy (NE). This work was performed to fulfill Level 2 Milestone M2SF-22OR010201042, "FY2021 ORNL Report on High Burnup Sibling Pin Testing Results," within work package SF-22OR01020104 and is an update to the work reported in M2SF-21OR010201032, M2SF-19OR0010201026 and M2SF-19OR010201028.

As a part of the DOE NE High Burnup Spent Fuel Data Project, Oak Ridge National Laboratory (ORNL) is performing destructive examinations (DEs) of high burnup (HBU) (>45 GWD/MTU) spent nuclear fuel (SNF) rods from the North Anna Nuclear Power Station operated by Dominion Energy [C-1]. The SNF rods, called the *sister rods* or *sibling rods*, are all HBU and include four different kinds of fuel rod cladding: standard Zircaloy-4 (Zirc-4), low-tin (LT) Zirc-4, ZIRLO, and M5. The DEs are being conducted to obtain a baseline of the HBU rod's condition before dry storage and are focused on understanding overall SNF rod strength and durability. Both fuel rods and empty cladding will be tested to derive material properties. Although the data generated can be used for multiple purposes, one primary goal for obtaining the postirradiation examination data and the associated measured mechanical properties is to support SNF dry storage licensing and relicensing activities by (1) addressing identified knowledge gaps and (2) enhancing the technical basis for post-storage transportation, handling, and consolidation activities.

This appendix documents the status of the ORNL Phase 1 DE activities [C-2, C-3] related to rod internal pressure and void volume measurement techniques, fission gas stack flow measurements applied to selected sister rods, and fission gas release calculations in Phase 1 of the sister rod test program.

Table CS-1 provides a summary of the results.

**Table CS-1. DE summary.**

Planned DE		Status	Comments
DE.01	Measure internal pressure of five baseline and three heat-treated rods	Complete	The rod internal pressure and the void volume available inside the rod were measured for eight sister rods at room temperature, and all pressures are within the publicly available database envelope. There is a clear correlation between the post-irradiated rod internal pressure and the as-designed fill pressure. The fission gas partial pressure trends well with the rod average burnup. The pressure and void volumes measured are consistent for rods from the same fuel vendor. The product of the partial pressure of the fission gas and the void volume, $P_f V$ , is consistent between ORNL and PNNL for sister rods from the same assembly, except for the two rods from assembly F35. A comparison of $P_f V$ indicates that the ZIRLO-clad rods might have experienced some change in pressure, void volume, or both due to the heat treatment applied, but the M5-clad rods do not exhibit the same effects. Comparisons with predictions from fuel rod performance codes FAST and BISON indicate a tendency for

Planned DE	Status	Comments
		FAST to underpredict pressure and BISON to overpredict pressure.
Measure rod void volume of five baseline and three heat-treated rods	Complete	<p>Eight rods were measured. All measured volumes are on the lower side of the publicly available database envelope but are consistent with other rods of their design type. By comparing the measured volumes of the baseline and heat-treated ZIRLO-clad rods, as well as the <math>P_fV</math> for all ZIRLO-clad sister rods, it appears that the heat treatment resulted in an increase in void volume. The heat-treated M5-clad rod is within measurement uncertainty of the baseline rod, and the heat-treatment did not appear to affect the void volume. No conclusions could be made about the effects of the heat-treatment on the Zirc-4-clad rod based on a comparison with the LT Zirc-4 baseline rod (because the LT Zirc-4 rod is batch fuel and the Zirc-4 rod was a lead test rod) or the Pacific Northwest National Laboratory Zirc-4-clad rod (because of differences in the measurement techniques). Comparisons with predictions from fuel rod performance codes FAST and BISON indicate a tendency for FAST to overpredict void volume and BISON to underpredict void volume.</p>
Measure the transmissibility of gas along the pellet stack	Complete	<p>Pellet stack gas transmissibility at room temperature was measured by using depressurization tests on eight rods and transmission tests on three rods. In all cases, gas was transmissible through the pellet stack at room temperature, requiring between 30 min and 24 h to reach equilibrium conditions, depending upon the pressure differential applied. The data correlates well using the Muskat-Poiseuille porous media method.</p> <p>The permeability of the pellet stack varied over less than one order of magnitude for this set of rods and could indicate some common feature about HBU fuel. Graphs of the data with burnup, lifetime maximum HDCI, and operating lifetime average assembly middle-of-cycle predicted fuel temperature indicate that the derived permeability is correlated to fuel operating temperature and maximum HDCI but is not correlated to the rod average burnup. The permeability does appear to be closely related to the rod's manufacturer, and the pellet manufacturing process might be important in determining the permeability of the pellet stack.</p> <p>Although the flow regimes associated with the pellet stack transmissibility did not change significantly for the heat-treated fuel rods, it appears that the heat treatments might have</p>

Planned DE		Status	Comments
			induced a shift to higher evaluated permeability. The role of the cladding in the resulting permeability shift is unclear.
	Calculate fission gas release fractions	Complete	The percentage of fission gas released from the pellets to the rod void space ranges from 1.5 to 3.5% for the rods punctured and are consistent with previously published data.

This page is intentionally blank

## ACKNOWLEDGMENTS

Many thanks to our US Department of Energy Office of Nuclear Energy sponsor, Ned Larson, along with the Spent Fuel and Waste Science and Technology (SFWST) storage and transportation program leadership for their continued support. The sister rod project would not have been possible without the vision and support of the Electric Power Research Institute, Westinghouse, Framatome, and Dominion Energy.

This work would not have been possible without the support and expertise provided by the leadership and staff members of the ORNL's Irradiated Fuel Examination Laboratory (IFEL). Special thanks go to Jerid Metcalf for his assistance with in-cell testing activities. Thanks go to Tracy Binger and Mark Walls for their quick support when radiation protection coverage was required during these tests.

Finally, we would like to express our gratitude to Ken Geelhood of PNNL for his detailed review of the rod internal pressure, void volume, and fission gas release data and the additional verification calculations he performed using FAST.

This page is intentionally blank



## CONTENTS

SUMMARY .....	iii
ACKNOWLEDGMENTS .....	vii
CONTENTS.....	ix
LIST OF FIGURES .....	xi
LIST OF TABLES .....	xiii
REVISION HISTORY .....	xv
ACRONYMS .....	xvii
C-1. Introduction .....	1
C-2. Puncture System Design, Operation, and Measurement Uncertainty.....	1
C-2.1 Puncture System Design and Operation.....	1
C-2.2 Calculation of Void Volume and Pressure.....	6
C-3. System Testing .....	8
C-3.1 Experimental Uncertainty Associated with the Measured Rod's Internal Pressure and Void Volume Measurements.....	10
C-3.2 Selection of Puncture System Hardware to Achieve Functionality while Minimizing Measurement Uncertainty .....	12
C-3.2.1 Example Puncture Device Behavior with a Fuel Rod.....	13
C-4. Residual Gas Effects.....	17
C-4.1 Estimated Time Required for Pumping out the Rod .....	17
C-4.2 Estimating the Volume of Gas that Could Be Trapped in the Pellet Stack following Rod Pump-Down.....	18
C-4.3 Effects on Rod Void Volume Determination if Gas is Trapped in the Pellet Stack .....	18
C-4.4 Impact of Different Rod and Reference Volume Temperatures .....	20
C-5. Depressurization and Gas Transmission Test Operation and Design Considerations.....	22
C-5.1 Data Analysis and Fitting.....	25
C-5.2 Application to Sealed Rods.....	26
C-6. Rod Internal Pressure and Void Volume Measurements of the Sister Rods .....	29
C-6.1 Comparisons of the Sister Rod Measured Internal Pressure and Void Volume with Available Data from Other Fuel Rods .....	29
C-6.2 Comparisons of the Measured Internal Pressure and Void Volume with Available Data from Other Sister Rods .....	34
C-6.3 Comparisons of the Heat-Treated Sister Rod Measured Internal Pressure and Void Volume with Baseline Sister Rods.....	38
C-6.4 Comparisons of the Measured Rod Internal Pressure and Void Volume with Code Predictions.....	40
C-7. Pellet Stack Gas Depressurization and Transmission Measurements of the Sister Rods .....	44
C-8. Fission Gas Release Calculations .....	51
REFERENCES .....	54

This page is intentionally blank

## LIST OF FIGURES

Figure C-1. Basic layout of the rod puncture apparatus used to measure rod internal pressure and void volume and to collect a sample of fission gas for analysis.....	3
Figure C-2. Illustration of the puncture housing (left) and a photo of a rod inserted into the housing for a rod internal pressure measurement (right). ....	4
Figure C-3. In-cell and out-of-cell components of the puncture apparatus. ....	5
Figure C-4. Pressure history of a rod puncture. ....	15
Figure C-5. Pressure history of a rod using the two-step method. ....	16
Figure C-6. System used to estimate the effects of small temperature differences between the fuel rod in the hot cell and the test control apparatus on the outside. ....	21
Figure C-7. Schematics of the depressurization and gas transmission test configurations. ....	23
Figure C-8. Rod inserted into the gas transmission support fixture with the pressure gauge and pressure supply line. ....	24
Figure C-9. Plenum end support brace in place to prevent the rod from moving forward. ....	24
Figure C-10. Sister rod measured rod internal pressure at 25°C.....	31
Figure C-11. Sister rod measured void volume 25°C with comparable historical data. ....	32
Figure C-12. Sister rod measured fission gas partial pressure at 25°C. ....	33
Figure C-13. Sister rod measured rod internal pressure vs. (a) measured rod void volume by manufacturer/cladding alloy, and (b) nominal beginning-of-life fill pressure of the rod by manufacturer/cladding alloy/parent assembly. ....	35
Figure C-14. Measured rod internal pressure as a function of various parameters of interest (red symbols denote heat-treated sister rods).....	36
Figure C-15. Calculated fission gas pressure as a function of various parameters of interest (red symbols denote heat-treated sister rods).....	37
Figure C-16. P/V as a function of burnup for (a) all data to date, (b) ZIRLO-clad sister rods, and (c) M5-clad sister rods.....	39
Figure C-17. BISON- and FAST-predictions vs. measured: (a) rod internal pressure, (b) void volume, (c) product of rod internal pressure and void volume (d) difference of predicted from measured by rod average burnup. ....	42
Figure C-18. Predicted rod internal pressure and void volume as compared with ORNL measurement data. ....	43
Figure C-19. Results of the depressurization tests on 8 sister rods (3 rods were heat-treated).....	45
Figure C-20. Results of gas transmission tests on 2 sister rods (3 different pressures on each rod). ....	46
Figure C-21. Pressure vs. time predictions using the Muskat-Poiseuille model for compressible gas flow and Darcy's law for incompressible flow for sister rod 3A1F05: depressurization (top) and gas transmission (bottom) test results. ....	48
Figure C-22. Evaluated Muskat-Poiseuille permeability for baseline rods subjected to transmission tests at various driving pressures by cladding type and heat-treatment.....	49

Figure C-23. Evaluated Muskat-Poiseuille permeability as a function of (a) rod average burnup, (b) assembly average fuel temperature during operation, (c) estimated rod HDCl, and (d) rod cladding type (also reflective of the rod manufacturer and vintage). .....	50
Figure C-24. The calculated percent fission gas release of the sister rods compared to open literature data [C-19] and [C-20]. .....	53

## LIST OF TABLES

Table CS-1. DE summary. ....	iii
Table C-1. Results of puncture apparatus testing. ....	9
Table C-2. Argon material properties used in calculations. ....	25
Table C-3. Results of rod internal pressure and void volume measurements at 25°C. ....	30
Table C-4. Summary of measured and predicted rod internal pressure and void volume. ....	41
Table C-5. Results of depressurization and transmission tests. ....	44
Table C-6. Calculated moles of Kr and Xe in gas after discharge. ....	52
Table C-7. Calculated percent fission gas released. ....	53

This page is intentionally left blank.

**REVISION HISTORY**

<b>Date</b>	<b>Changes</b>
3/29/2019	Initial release
9/27/2019	Revised to include additional data and incorporate comments from the previously released report.
10/29/2020	Moved the detailed description of the test apparatus to this appendix. Made changes to text as needed to re-sequence the information.  Moved the detailed measurement results and data comparisons to this appendix. Made changes to the text as needed to re-sequence the information.
11/30/2020	The document numbering was revised to reflect its M2 status, and the date was changed.
10/29/2021	Section C-8 was added to calculate the fission gas release terms. Minor editorial changes were made throughout.
3/31/2022	The document number was revised to reflect its M2 status and inclusion in the FY21 report and the date was changed.

This page is intentionally left blank.



## ACRONYMS

DE	destructive examination
DOE	US Department of Energy
EPRI	Electric Power Research Institute
FHT	full length rod heat treatment
HBU	high burnup
HDCI	high duty core index
ID	inner diameter
IFBA	integral fuel burnable absorber
LT	low tin
NE	Office of Nuclear Energy
OD	outer diameter
ORNL	Oak Ridge National Laboratory
PCI	pellet-cladding interaction
PNNL	Pacific Northwest National Laboratory
PWR	pressurized water reactor
SNF	spent nuclear fuel

This page is intentionally left blank.

## C-1. Introduction

Commercial nuclear fuel rods are pre-pressurized with helium before irradiation. The magnitude of pre-pressurization varies with fuel design; at manufacture, the sister rods were pre-pressurized between 1.7 and 2.5 MPa, depending upon their design. Each fuel rod includes a spring in a plenum at the top of the rod to provide a small compression load on the fuel pellet stack inside the rod, mainly to ensure that gaps between pellets do not occur. During irradiation and subsequent storage, the rod internal pressure increases due to a production of fission gases (e.g., xenon, krypton) and volumetric changes caused by pellet swelling and clad irradiation growth. At manufacture, the rod includes spaces that are unoccupied by the fuel stack and spring, termed the *void volume*. In this discussion, the *void volume* is defined as including the volume in the plenum of the rod that is not occupied by the spring, the gap between the pellet outer diameter (OD) and the cladding inner diameter (ID), the volume of any pellet chamfers and dishes, and the volume of pellet cracks and open porosity at the specified temperature. The void volume changes during operation as the cladding creeps and grows as a result of irradiation and as cracks and porosity are formed within the pellets. Because rod internal pressure and void volume are important parameters in determining the rod's performance throughout its lifetime, both were measured for each sister rod.

This appendix provides detailed information on the design and testing of the systems used to measure rod internal pressure, void volume, and gas transmissibility through the pellet stack.

## C-2. Puncture System Design, Operation, and Measurement Uncertainty

This section describes in detail the puncture system design and its operation, as well as derivation of the  $2\sigma$  measurement uncertainties, a description of the out-of-cell testing performed, discussions on the time required to pump down a fuel rod to vacuum, estimated retained fission gas volumes after rod pump-down, and calculated impacts of retained fission gas and temperature differentials on the final pressure and volume measurements for the Oak Ridge National Laboratory (ORNL) system. The measurement system's design is extremely important for achieving accurate internal rod pressure and void volume measurements.

To measure the gas pressure and void volume of a fuel rod, the plenum region of the rod is punctured, and the ideal gas law, in conjunction with known pressures and volumes, is used to determine the results. The plenum end of the fuel rod is sealed into an evacuated housing of known volume—the *tare* volume. After puncture, the pressure in the housing is measured, and then the gas is expanded into another chamber of known volume, and the new pressure is measured. This double expansion method allows the rod's internal pressure and free internal volume to be determined in one operation. Once measurements are completed, the housing and the now-accessible free rod volume are evacuated and backfilled with a known volume and pressure of gas, and the final gas pressure is measured. This process allows for a second two-step measurement of the rod's void volume and a second calculation for the rod's internal pressure for comparison with the first method.

### C-2.1 Puncture System Design and Operation

The basic layout of the puncture apparatus is shown in Figure C-1, and the puncture housing is shown in Figure C-2; an overview of both is shown in Figure C-3. Only part of the apparatus is in the hot cell; the radiation-sensitive gauge, fission gas sample bottle, inert gas supply, and vacuum pump are all outside the hot cell. Like many of the components, the line connecting the pressure gauge to the puncture housing has a small diameter to minimize volume because minimizing the tare volume is an important system

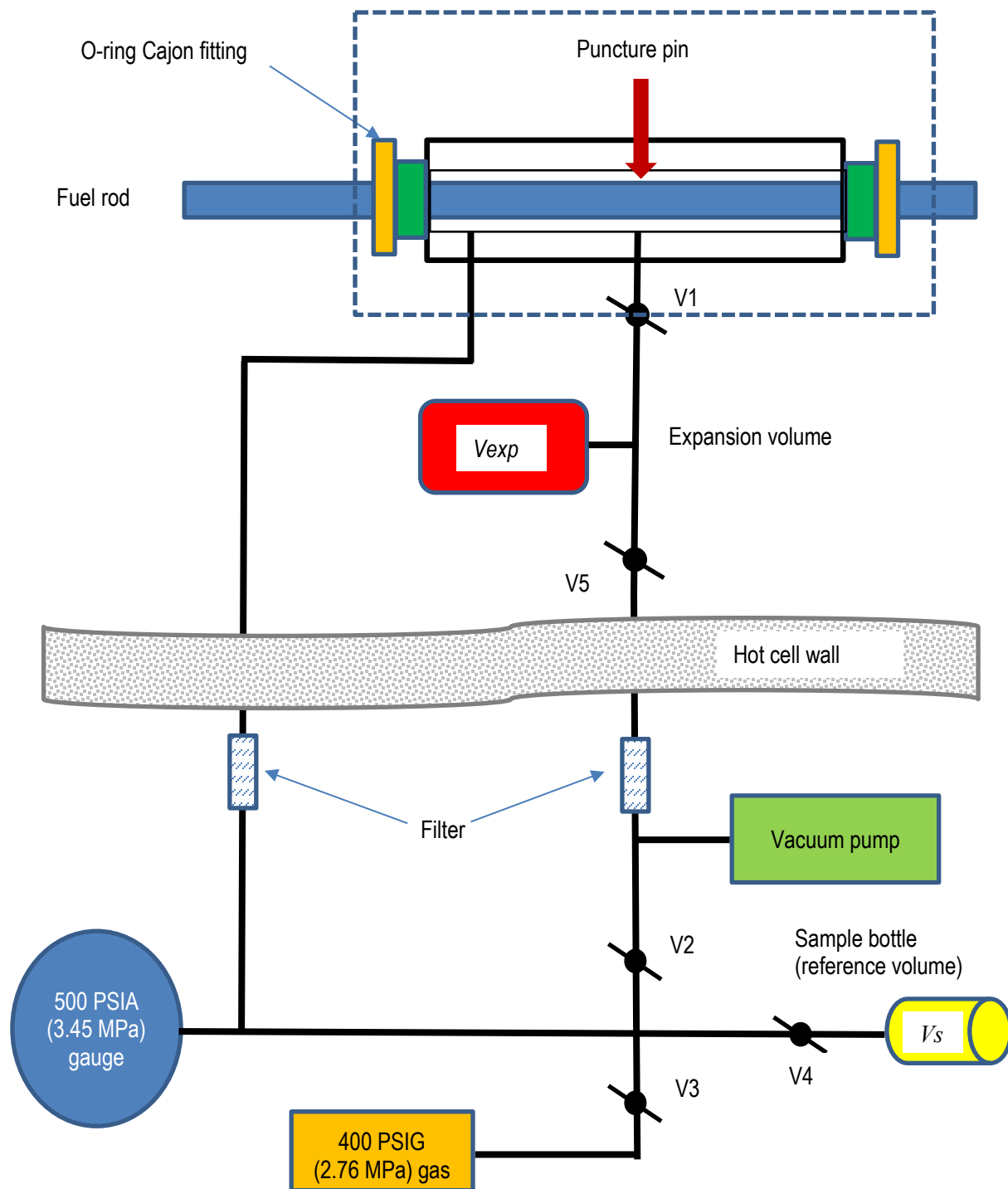
consideration. Component sizes were optimized based on the uncertainties in the system's reference volumes and pressure indicator.

To operate the puncture system, the plenum end of the fuel rod is inserted into the puncture unit and sealed within the puncture housing, as shown in Figure C-1. The small clearance between the OD of the rod and the ID of the puncture housing becomes a part of the system's tare volume. Before measurements are made, system seals are checked by holding pressure and then by holding vacuum. Once a leak-free system has been demonstrated, the tare volume is measured. Because the accuracy of the rod internal pressure and void volume measurements are very sensitive to the total system volume, the tare volume must be measured individually and accurately for each fuel rod. This is done by evacuating the tare volume and then expanding a known pressure and volume of inert gas (argon) into the tare volume. The fission gas sample bottle is used as a reference standard, providing a known pressure and volume of inert gas for the measurement. The volume of each fission gas sample bottle is individually measured before use (nominally 26 cc) and is known within  $\pm 0.2$  cc. After expanding the inert gas from the fission gas sample bottle to the evacuated system's tare volume, the ideal gas law can be used to calculate the system's tare volume (nominally 25 cc). Temperature is monitored during the measurements, and the calculations include temperature adjustments, as required.

Once the system tare volume is known, the rod is punctured within the housing in the following sequence: (1) the tare volume and the volume of a second calibrated volume bottle, the *expansion volume* (29.3 cc) are evacuated; (2) the expansion volume is valved off; and (3) the sharpened point of the puncture pin is advanced until a pressure increase is detected by the pressure gauge. After puncture, the rod's free fission gas expands from the rod's void volume to fill the system's tare volume, and the pressure is recorded. The valve to the expansion volume is then opened, and the fission gas sample is expanded a second time into the known expansion volume. The final pressure is then recorded, and the ideal gas law is used to calculate the rod's internal pressure and void volume using the two measured pressure values and the known expansion and tare volumes. This is called the *double expansion method*. The double expansion method generally has a slightly higher measurement uncertainty than the *two-step method* that is related to the inclusion of one additional uncertainty associated with the second expansion operation. In practice, the double expansion and two-step methods are complimentary because they provide independent corroborating data and an independent check on the operation of the apparatus.

Next, to capture a fission gas sample, the system pressure is reduced to ensure that the sample dose is low enough for transfer outside the hot cell. To achieve this, the puncture pin is backed out of the housing enough to vent some of the fission gas to the hot cell's atmosphere. At a pressure reading of  $\sim 16$  psia (0.11 MPa), which is slightly above local atmospheric pressure, the pin is again advanced into the housing to seal it, and the valve to the fission gas sample volume is opened. This low-pressure fission gas sample is expected to have the same mole ratio of gases that the original mixture contained within the fuel rod plenum, and the total number of gas moles can be calculated based on the measured total system volume and pressure.

Finally, to keep the rod's void volume measurement uncertainty as low as possible as it is further propagated into the rod's internal pressure measurement, a two-step method that leverages the smaller fission gas sample bottle volume is used. After obtaining the fission gas sample, the rod and puncture system are evacuated. A second (i.e., replacement) fission gas sample bottle is pressurized using an inert gas at a known pressure and known volume. This gas is then expanded into the evacuated tare and fuel rod void volume. This provides a second method of determining the rod's void volume and pressure, which can be compared with the double expansion method. Temperature is monitored during the measurements, and the volume and pressure measurements are standardized to 25°C.



*Note: only part of the apparatus is in the hot cell. The sample bottle provides a reference volume, and it also serves as a removable gas sample to be sent to the radiochemical laboratory.*

**Figure C-1. Basic layout of the rod puncture apparatus used to measure rod internal pressure and void volume and to collect a sample of fission gas for analysis.**

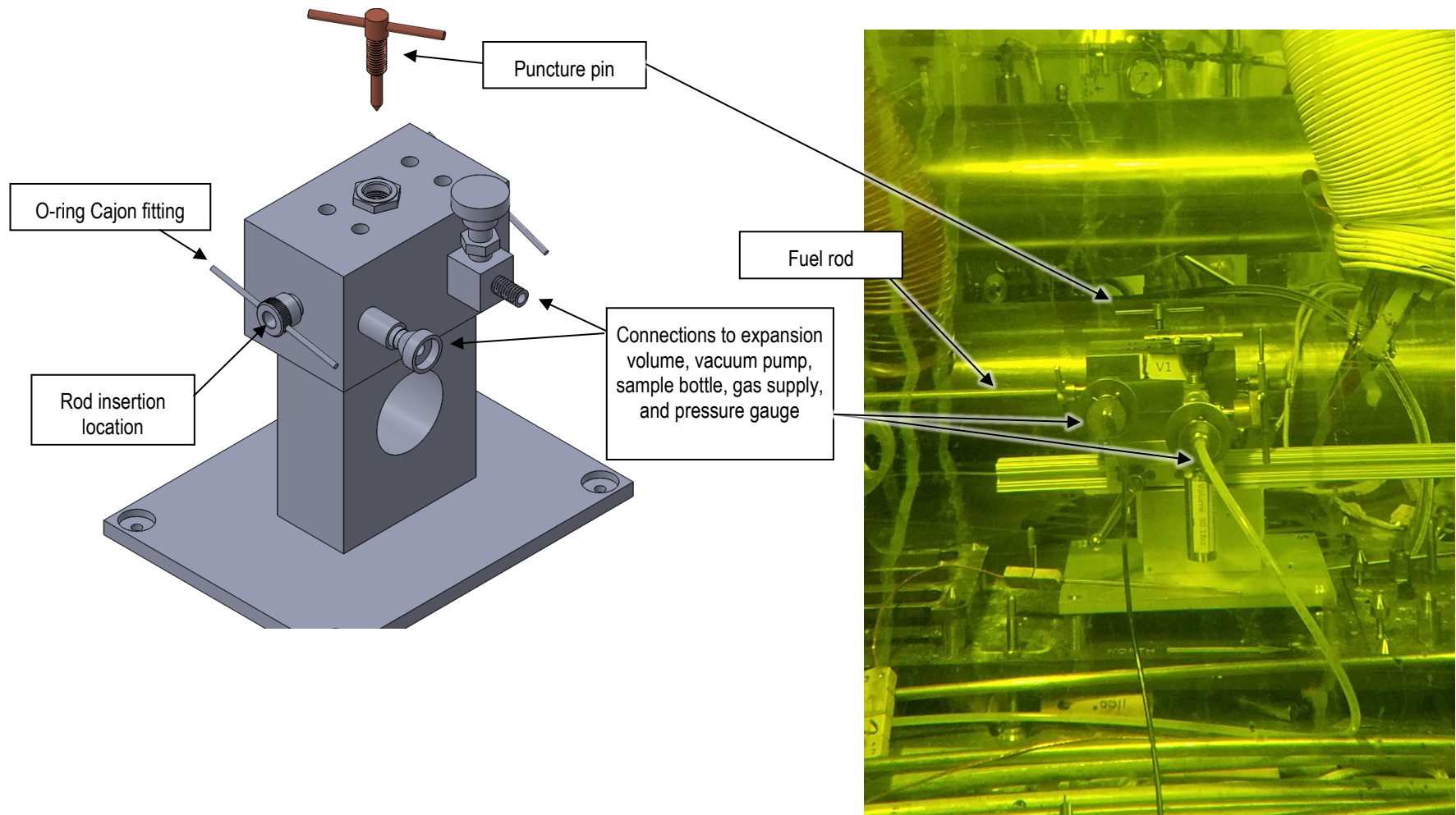
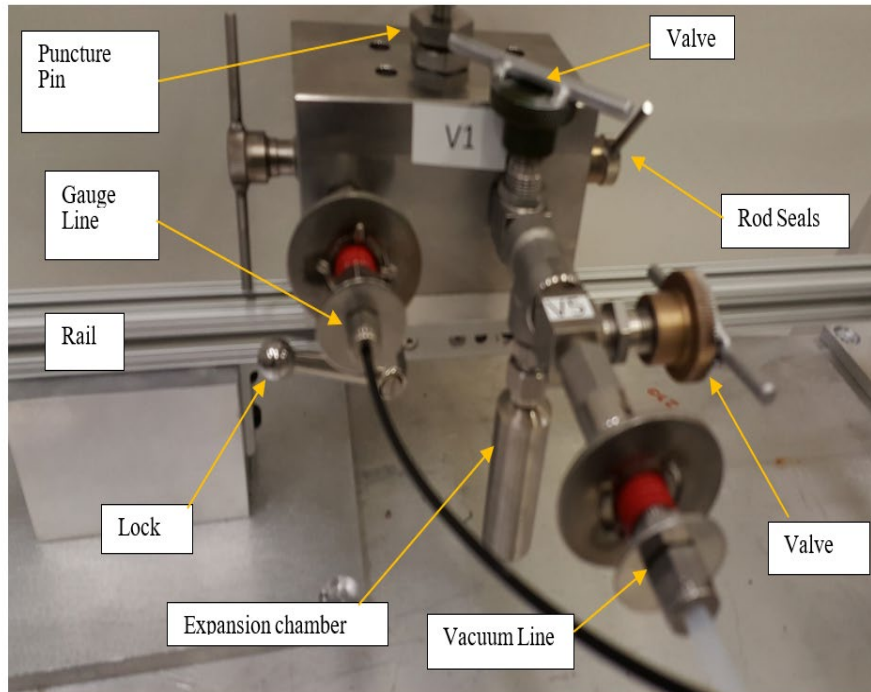
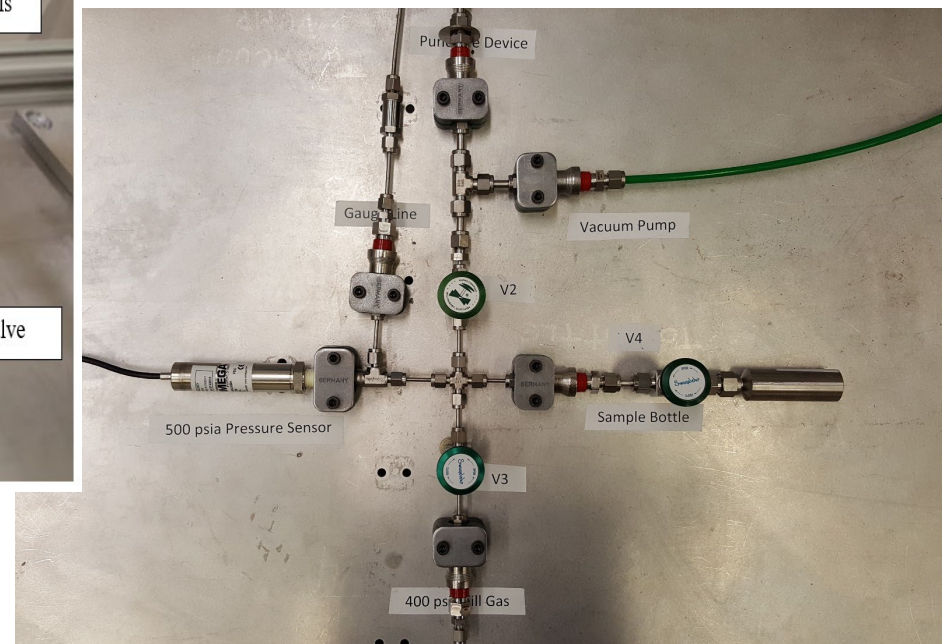


**Figure C-2. Illustration of the puncture housing (left) and a photo of a rod inserted into the housing for a rod internal pressure measurement (right).**





In-cell portion of the puncture apparatus containing the control valves, puncture pin, and expansion chamber.



Out-of-cell portion of the puncture apparatus containing the control valves, pressure sensor, and sample bottle.

Figure C-3. In-cell and out-of-cell components of the puncture apparatus.

## C-2.2 Calculation of Void Volume and Pressure

Throughout the puncture process, gas is redistributed within the puncture system and the rod being punctured. It is necessary to pause at each redistribution event to allow for stabilization time. Stabilization is monitored at each gas redistribution event using the system gauge and is considered to be achieved when the pressure change that occurs over a few seconds is small ( $<0.1$  psig [0.7 kPa]).

### Step 1: Determine puncture system tare volume.

To determine the system's tare volume (i.e., the volume of the apparatus and connecting lines),  $V_t$ , the fuel rod is inserted into the puncture unit and sealed by tightening the Cajon fittings. The system is then checked for leaks, both under vacuum and pressure.

Next, valves V1, V2, V4, and V5 are opened, and the system is pumped down to vacuum. Valves V1 and V2 are then closed, and V3 is opened to fill the fission gas sample bottle, system connecting lines, and clearance between the fuel rod and puncture housing with inert gas at  $\sim 415$  psia (2.86 MPa). The expansion volume, which was determined from previous out-of-cell measurements, and the vacuum pump are valved out of the system. Valves V3 and V4 are then closed, and the system pressure is recorded. V1 and V2 are then opened, and the system is pumped down to vacuum. The fission gas sample bottle valve is not opened, and the recorded pressure is retained in the fission gas sample bottle's known volume. Once a stable vacuum is reached, V1 and V2 are closed. Finally, V4 is opened, expanding the known pressure and volume of inert gas from the fission gas sample bottle to the system volume. The system pressure is recorded after a few seconds, once the system has stabilized. Because the puncture unit and connecting lines are brought down to vacuum—except for the sample bottle ( $V_s$ ), which has a known volume—the moles of gas in the system at the sample bottle starting pressure ( $P_{st}$ ) for a constant temperature are determined by using the ideal gas law  $PV = nRT$ , as follows:

$$P_{st}V_s. \quad (C-1)$$

When valve V4 is opened, the sample bottle's ending pressure  $P_{et}$  is lower because the gas expands to fill both the bottle and the tare volume ( $V_t$ ) (constant temperature) so that the moles of gas in each volume sum to the total:

$$P_{st}V_s = P_{et}(V_s + V_t). \quad (C-2)$$

Solving gives

$$V_t = V_s \left( \frac{P_{st}}{P_{et}} - 1 \right). \quad (C-3)$$

The known volumes of all sample bottles are measured before use.

### Step 2: Collect puncture data.

To puncture a rod, valves V1, V2, V4, and V5 are first opened to pump the system down to vacuum. Then, all four valves are closed, and the sharp end of the puncture pin is slowly advanced to punch the rod cladding. Penetration is observed by a jump in system pressure; the pin is then backed out a small amount to allow an unimpeded gas path. Once the pressure stabilizes over several minutes or more, the pressure,  $P_{pun}$ , is recorded. Next, valve V1 is opened, and the system pressure is allowed to stabilize over several minutes or more, usually for a longer amount of time than allowed for the first measurement. This new pressure,  $P_{exp}$ , is recorded. If the pressure is greater than 16 psia (0.11 MPa), then the punch pin is slowly unscrewed to allow gas to escape the puncture unit until the pressure is about 16 psia (0.11 MPa). The pin is then screwed back in, and the system is allowed to stabilize for much longer than the previous times, and this pressure is then recorded as  $P_{sys}$ . Valve V4 is then opened to capture a gas sample; when the pressure stabilizes, it is recorded as  $P_{bot}$ .



At this point, enough data are available to calculate the rod's void volume and internal pressure using the *double expansion* method. Since the puncture unit and connecting lines were evacuated, the moles of gas in the system at the rod volume  $V_p$  and the rod pressure  $P_p$  for a constant temperature are determined by

$$P_p V_p. \quad (C-4)$$

When the rod is punctured, the pressure  $P_p$  drops as the gas expands to fill the tare volume ( $V_t$ ), and the system pressure (constant temperature) drops so that the moles of gas in each volume sum to the total:

$$P_p V_p = P_{pun}(V_p + V_t). \quad (C-5)$$

When V1 is opened to allow the gas to flow into the expansion volume ( $V_{exp}$ ), the pressure drops even more, resulting in

$$P_p V_p = P_{exp}(V_p + V_t + V_{exp}). \quad (C-6)$$

Equations (C-5) and (C-6) can be solved for  $P_p$  and  $V_p$ :

$$V_p = \frac{P_{exp} V_{exp}}{(P_{pun} - P_{exp})} - V_t, \text{ and} \quad (C-7)$$

$$P_p = \frac{P_{pun}(V_p + V_t)}{V_p}. \quad (C-8)$$

### Step 3: Collect a fission gas sample for analysis.

To capture a fission gas sample, first it is necessary to reduce the system pressure to ensure that the fission gas sample dose will be low enough for transfer outside the hot cell. To achieve this, the puncture pin is backed out of the housing enough to vent some of the fission gas to the hot cell's atmosphere, as previously noted. At a pressure reading of ~16 psia (0.11 MPa), which is slightly above local atmospheric pressure, the pin is again advanced into the housing to seal it, and the valve to the fission gas sample volume is opened. This low-pressure fission gas sample is expected to have the same mole ratio of gases as the original mixture contained within the fuel rod plenum, and the total number of gas moles can be calculated based on the measured total system volume and pressure.

When V4 is opened to the fission gas sample bottle at constant pressure and temperature, the moles of gas are distributed via the volume fraction. When the pressure is bled off, the amount in the bottle is the fraction of the new pressure over the original pressure. This gives

$$F = \frac{V_s}{(V_p + V_t + V_s + V_{exp})} \frac{P_{sys}}{P_{exp}}. \quad (C-9)$$

### Step 4: Perform the two-step method to measure the rod void volume.

As a complementary measurement to the double expansion method outlined in Step 2, after the rod is punctured and the fission gas is removed, the rod's volume can be determined using a process similar to that used to measure the tare volume. The tare volume and fuel pin's void volume ( $V_p$ ) are evacuated. A fission gas sample bottle ( $V_s$ ) is pressurized with an inert gas ( $P_{sp}$ ), and the number of moles for a constant temperature is

$$P_{sp} V_s. \quad (C-10)$$

When the valve to the remainder of the puncture system is opened, the inert gas expands to fill the tare volume and the spent fuel rod's void volume. Using the ideal gas law (assuming constant temperature), the relationship between the starting and ending pressures can be related to the system volumes of

interest, as follows:

$$P_{sp}V_s = P_{ep}(V_s + V_p + V_t). \quad (C-11)$$

Solving gives

$$V_p = V_s \left( \frac{P_{sp}}{P_{ep}} - 1 \right) - V_t. \quad (C-12)$$

Thus, the two-step method eliminates some uncertainties from the measurement by eliminating the reliance on the measured puncture pressure in favor of the known inert gas pressure and by using the smaller fission gas sample bottle instead of the larger expansion volume. The rod's internal pressure is reevaluated by using the two-step method for rod internal volume:

$$P_p = \frac{P_{pun}(V_p + V_t)}{V_p}. \quad (C-13)$$

However, the system's tare volume remains an important term in the calculation that must be specifically measured for each rod punctured. Additionally, the incomplete evacuation of fission gas trapped within the fuel stack influences the result.

Two steps are necessary before the equations can be solved: (1) the fuel pin is punctured and the puncture values are recorded, and (2) the pin is backfilled to determine the volume,  $V_p$ . This two-step process contrasts with the double expansion method, which uses a second expansion to provide the information needed to determine both rod pressure and volume in a coupled system of equations. By using both methods, results can be checked to ensure consistency and to reduce uncertainty.

### C-3. System Testing

The puncture apparatus was designed and fabricated using estimated design parameters. The as-fabricated apparatus is slightly different in actual measurement, but it is reasonably close so that the uncertainty estimates are not markedly different. The design goal was to achieve a 4–6%  $2\sigma$  uncertainty range.

As an example, the as-fabricated values for one set of reference volumes are as follows:

$$\begin{aligned} V_{ref} &= 26.1 \text{ cc (typical, several were used and transferred to the radiochemical laboratory)} \\ \Delta V_{ref} &= 0.21 \text{ cc} \\ V_{exp} &= 29.34 \text{ cc} \\ \Delta V_{exp} &= 0.23 \text{ cc} \\ V_{tare} &= 25 \text{ cc (typical, varies with test)} \\ P_{fill} &\approx 400 \text{ psia (2.76 MPa) (varied somewhat between tests, actual value used)} \end{aligned}$$

Each reference volume was determined by filling the containers with water and weighing them three or more times. The volume of the expansion chamber was slightly refined by using the test rod specimens to reduce an unavoidable assembly tolerance.

To test the functionality of the system and verify the uncertainty estimates, ORNL procured 12 stainless-steel surrogate pins for puncture. The pins were all  $\frac{3}{8}$  in. in diameter and ranged from 7 to 10 in. long to simulate the expected range of rod void volume. They were pressurized between 500 to 1,500 psia (3.45 to 10.34 MPa) to simulate the expected range of pressure using an inert gas. Five surrogates were punctured out of cell, and three others were punctured in cell. The remainder of the surrogate rods are being held in reserve and will be used when additional punctures of the sister rods are completed to verify system functionality (Table C-1).

Table C-1. Results of puncture apparatus testing.

Test	Fabricated pressure corrected for temperature (psia) <1%	Fabricated volume (cc) <1%	Measured volume, double expansion method (cc)	Volume difference, double expansion method	Measured pressure, double expansion method (psia)	Pressure difference, double expansion method (%)	Measured volume, two-step method (cc)	Volume difference, two-step method (%)	Measured pressure, two-step method (psia)	Pressure difference, two-step method (%)	Comments
Test01a	495	10.48	9.91	-5.4%	490	-1.1	10.39	-0.9	474	-4.4	Lowest pressure
Test02	993	7.86	7.54	-4.1%	904	-9.0	7.83	-0.4	878	-11.6	Smallest volume, suspect specimen leak
Test03	494	9.17	8.56	-6.7%	498	0.7	9.22	0.6	471	-4.7	Lowest pressure
Test04	1,475	11.79	11.77	-0.2%	1,470	-0.3	11.72	-0.6	1,475	0.0	Largest volume
Test05	987	11.79	11.42	-3.1%	982	-0.5	11.76	-0.2	962	-2.5	Largest volume
Test06	1,474	7.86	7.83	-0.4%	1,505	2.1	8.09	3.0	1,467	-0.5	Smallest volume
HT01	998	10.48	10.49	0.1%	972	-2.6	10.59	1.0	966	-3.2	In hot cell
HT03	502	11.79	11.27	-4.4%	488	-2.7	11.47	-2.7	481	-4.1	In hot cell
Test07	506	7.86	7.37	-6.2%	494	-2.2	7.83	-0.3	471	-6.8	In hot cell

### C-3.1 Experimental Uncertainty Associated with the Measured Rod's Internal Pressure and Void Volume Measurements

To optimize the puncture system, the experimental uncertainty is derived and quantified. Furthermore, the pellet stack introduces a flow impedance into the system that must be considered to estimate the pressure stabilization time, which is a function of pressure.

The  $2\sigma$  uncertainty associated with the rod's internal pressure and void volume measurements can be estimated by taking the square-root-sum-squares of the partial derivatives of the appropriate variable multiplied by its measurement uncertainty (negligible measurement correlation).

For example, for the uncertainty associated with the two-step rod void volume,  $V_p$ , the measurement can be evaluated as follows:

$$V_p = V_s \left( \frac{P_{sp}}{P_{ep}} - 1 \right) - V_t, \quad (C-14)$$

$$\frac{\partial V_p}{\partial V_s} = \frac{P_{sp}}{P_{ep}} - 1, \quad (C-15)$$

$$\frac{\partial V_p}{\partial P_{sp}} = \frac{V_s}{P_{ep}}, \quad (C-16)$$

$$\frac{\partial V_p}{\partial P_{ep}} = -V_s \frac{P_{sp}}{P_{ep}^2}, \text{ and} \quad (C-17)$$

$$\frac{\partial V_p}{\partial V_t} = -1, \quad (C-18)$$

and the uncertainty of the rod void volume measurement can be estimated as

$$\Delta V_p = \left[ \left( \frac{\partial V_p}{\partial V_s} \Delta V_s \right)^2 + \left( \frac{\partial V_p}{\partial P_{sp}} \Delta P_{sp} \right)^2 + \left( \frac{\partial V_p}{\partial P_{ep}} \Delta P_{ep} \right)^2 + \left( \frac{\partial V_p}{\partial V_t} \Delta V_t \right)^2 \right]^{1/2}. \quad (C-19)$$

The pressure gauge accuracy, volume of the fission gas sample bottle, and system tare volume are significant factors within the equation. The form of the rod void volume's uncertainty can be rewritten in terms of the parameters of interest:

$$\Delta V_p = \left[ \left( (V_p + V_t) \frac{\Delta V_s}{V_s} \right)^2 + \left( (V_p + V_t + V_s) \frac{\Delta P_{sp}}{P_{sp}} \right)^2 + \left( \frac{(V_p + V_t + V_s)^2}{V_s} \frac{\Delta P_{ep}}{P_{sp}} \right)^2 + (\Delta V_t)^2 \right]^{1/2}. \quad (C-20)$$

In this form, it can easily be observed that the system tare volume, fission gas sample bottle volume, and pressure gauge uncertainty are the primary parameters to be controlled and minimized in the puncture system design.

For the double expansion method, the uncertainty of the rod void volume measurement is different:

$$V_p = \frac{P_{exp} V_{exp}}{(P_{pun} - P_{exp})} - V_t, \quad (C-21)$$

$$\frac{\partial V_p}{\partial V_t} = -1, \quad (C-22)$$

$$\frac{\partial V_p}{\partial V_{exp}} = \frac{P_{exp}}{(P_{pun} - P_{exp})}, \quad (C-23)$$

$$\frac{\partial V_p}{\partial P_{exp}} = \frac{V_{exp} P_{pun}}{(P_{pun} - P_{exp})^2}, \text{ and} \quad (C-24)$$

$$\frac{\partial V_p}{\partial P_{pun}} = -\frac{V_{exp} P_{exp}}{(P_{pun} - P_{exp})^2}, \quad (C-25)$$

and the uncertainty of the rod void volume measurement can be estimated as

$$\Delta V_p = \left[ \left( \frac{\partial V_p}{\partial V_t} \Delta V_t \right)^2 + \left( \frac{\partial V_p}{\partial V_{exp}} \Delta V_{exp} \right)^2 + \left( \frac{\partial V_p}{\partial P_{exp}} \Delta P_{exp} \right)^2 + \left( \frac{\partial V_p}{\partial P_{pun}} \Delta P_{pun} \right)^2 \right]^{1/2}. \quad (C-26)$$

Again, the uncertainty can be written in terms of the parameters of interest:

$$\Delta V_p = \left[ (\Delta V_t)^2 + \left( (V_p + V_t) \frac{\Delta V_{exp}}{V_{exp}} \right)^2 + \left( \frac{(V_p + V_t)(V_p + V_t + V_{exp})^2}{P_p V_p V_{exp}} \Delta P_{exp} \right)^2 + \left( \frac{(V_p + V_t)^2 (V_p + V_t + V_{exp})}{P_p V_p V_{exp}} \Delta P_{pun} \right)^2 \right]^{1/2}. \quad (C-27)$$

By inspection, the important parameters to control and minimize are the expansion volume uncertainty, system tare volume, and pressure gauge uncertainty.

The uncertainty of the rod's internal pressure measurement,  $P_p$ , for the double expansion and two-step methods is

$$P_p = \frac{P_{pun}}{V_p} (V_p + V_t), \quad (C-28)$$

$$\frac{\partial P_p}{\partial P_{pun}} = 1 + \frac{V_t}{V_p}, \quad (C-29)$$

$$\frac{\partial P_p}{\partial V_t} = \frac{P_{pun}}{V_p}, \text{ and} \quad (C-30)$$

$$\frac{\partial P_p}{\partial V_p} = -P_{pun} \frac{V_t}{V_p^2}, \quad (C-31)$$

and the uncertainty of the rod internal pressure measurement can be estimated as

$$\Delta P_p = \left[ \left( \frac{\partial P_p}{\partial P_{pun}} \Delta P_{pun} \right)^2 + \left( \frac{\partial P_p}{\partial V_t} \Delta V_t \right)^2 + \left( \frac{\partial P_p}{\partial V_p} \Delta V_p \right)^2 \right]^{1/2}. \quad (C-32)$$

Rewriting in terms of the parameters of interest gives

$$\Delta P_p = \left[ \left( \left( 1 + \frac{V_t}{V_p} \right) \Delta P_{pun} \right)^2 + \left( \frac{P_p}{(V_p + V_t)} \Delta V_t \right)^2 + \left( \frac{P_p V_t}{V_p (V_p + V_t)} \Delta V_p \right)^2 \right]^{1/2}. \quad (C-33)$$

The pressure gauge uncertainty and system tare volume are important factors to ensure that the puncture system is designed with minimal uncertainty. Also, since the measured rod's void volume is included in the  $2\sigma$  uncertainty, all the terms associated with the rod's void volume must also be considered.

### C-3.2 Selection of Puncture System Hardware to Achieve Functionality while Minimizing Measurement Uncertainty

Based on the system's uncertainty analysis, the system's tare volume must be minimized to reduce measurement uncertainty for the rod's internal pressure and void volume. However, the puncture system lines must reach from the fuel rod plenum location in the hot cell to the pressure gauge and sample bottles outside the cell, and the length of the tubing and valve volumes primarily dictate the required minimum system tare volume. Therefore, there is a lower limit to the system's tare volume associated with the cell requirements, and the expected tare volume is ~25 cc.

To select the appropriate sizes for the other critical system features—the fission gas sample bottle, the expansion volume, the inert gas pressure, and the pressure gauge uncertainty—the terms within the uncertainty expressions were further expanded, and the sensitivity was evaluated.

For example, the uncertainty associated with the system tare volume,  $V_t$ , measurement, can be evaluated as described in the previous section:

$$V_t = V_s \left( \frac{P_{st}}{P_{et}} - 1 \right), \quad (C-34)$$

$$\frac{\partial V_t}{\partial V_s} = \frac{P_{st}}{P_{et}} - 1, \quad (C-35)$$

$$\frac{\partial V_t}{\partial P_{st}} = \frac{V_s}{P_{et}}, \text{ and} \quad (C-36)$$

$$\frac{\partial V_t}{\partial P_{et}} = -V_s \frac{P_{st}}{P_{et}^2}, \quad (C-37)$$

and the uncertainty of the system tare volume measurement can be estimated as

$$\Delta V_t = \left[ \left( \frac{\partial V_t}{\partial V_s} \Delta V_s \right)^2 + \left( \frac{\partial V_t}{\partial P_{st}} \Delta P_{st} \right)^2 + \left( \frac{\partial V_t}{\partial P_{et}} \Delta P_{et} \right)^2 \right]^{1/2}. \quad (C-38)$$

Rewriting in terms of the parameters of interest results in

$$\Delta V_t = \left[ \left( V_t \frac{\Delta V_s}{V_s} \right)^2 + \left( (V_s + V_t) \frac{\Delta P_{st}}{P_{st}} \right)^2 + \left( \frac{(V_s + V_t)^2}{V_s} \frac{\Delta P_{et}}{P_{st}} \right)^2 \right]^{1/2}. \quad (C-39)$$

Because  $V_t$  is fixed in practice, a reduction in the uncertainty measurement relies on a large starting pressure. The denominator of the expression generally includes the volume of the fission gas sample bottle, but it is also present in the numerator.

Therefore, to design the puncture device, the volumes  $V_s$  and  $V_{exp}$  were selected to minimize the uncertainties and to ensure that the before and after pressure readings would be in the gauge range. The tare volume of the apparatus and connecting lines were fabricated to be as small as practical.

Sensitivity studies were conducted for the fission gas sample bottle volume, expansion volume, inert gas pressure, and pressure gauge uncertainty to select an optimum combination for use in the puncture system. Based on available hardware, the starting point for the optimization was as follows:

$$V_t = 25 \text{ cc (fixed based on tubing and valving requirements)}$$

$$P_{st} = 400 \text{ psia (2.76 MPa)}$$

$$\Delta P_{sp} = \Delta P_{ep} = 0.4 \text{ psia (2.8 kPa)}$$

$$V_s = 25 \text{ cc (based on available sizes)}$$

$$\Delta V_s = 0.01 * V_s \text{ cc}$$

$$V_{exp} = 20 - 60 \text{ cc (based on available sizes)}$$

$$\Delta V_{exp} = 0.01 * V_{exp} \text{ cc}$$

In a practical device, the actual values for  $V_s$  and  $V_{exp}$  are compromise values.

### C-3.2.1 Example Puncture Device Behavior with a Fuel Rod

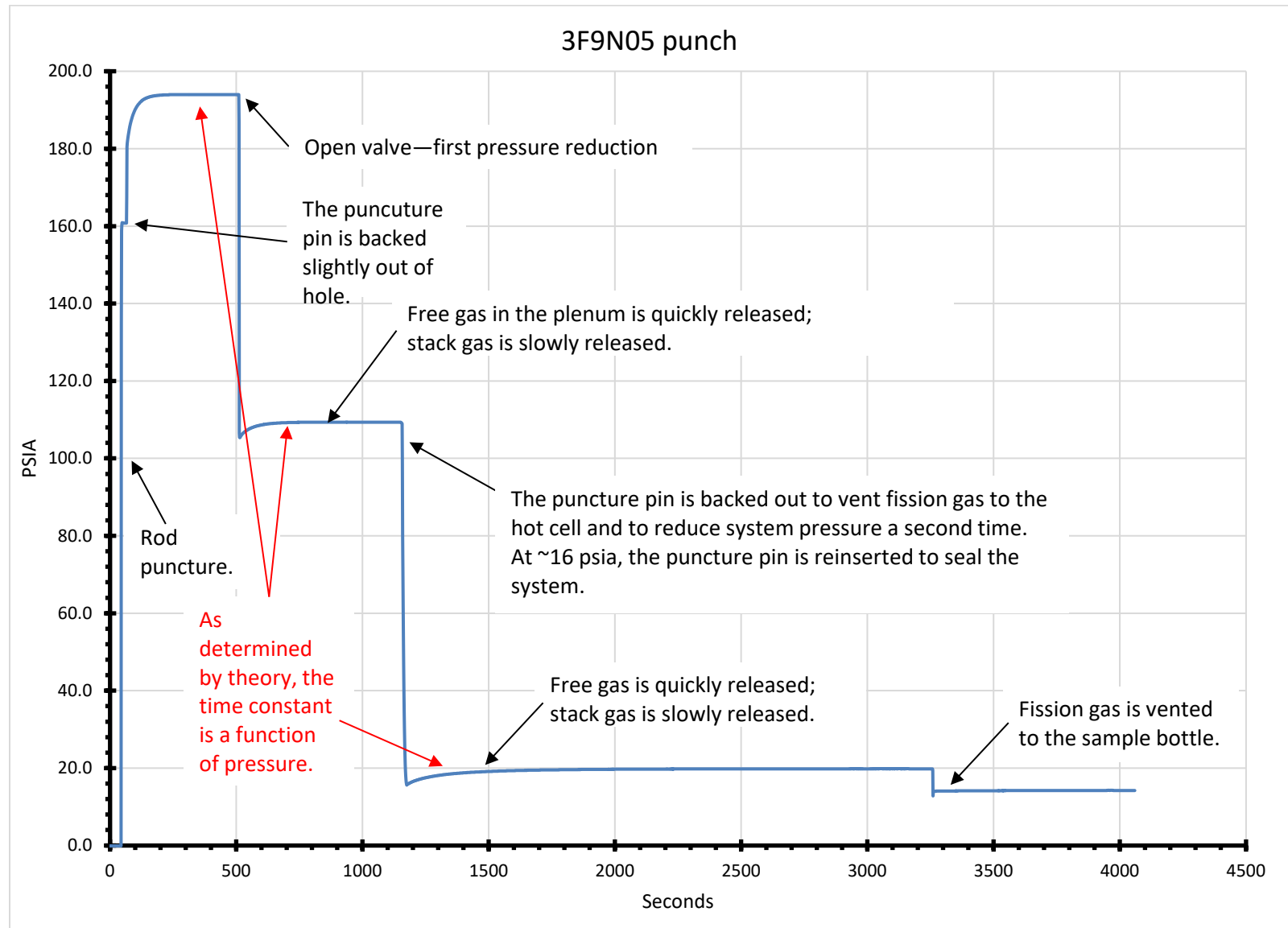
An example of fuel rod gas transmission behavior during the puncture phase can be seen by examining the pressure history of sister rod 3F9N05. As shown in Figure C-4, after puncture, the expansion of the gas in the plenum is relatively quick. The expansion of gas from the pellet stack is slower, and some time is required until an equilibrium is reached. Next, the valve to the expansion chamber is opened, and the pressure quickly drops, followed by a slight rise in pressure as the pellet stack gas expands, with equilibrium requiring a noticeably longer time. After the punch is opened to relieve the gas pressure and is then closed, the pressure slowly increases as more gas works its way through the stack over a much longer time. Finally, the valve to the sample bottle is opened and allowed to reach equilibrium again. The final equilibrium state can be difficult to resolve since, consistent with theory, the time constant is longer for the lower pressures. This demonstrates why it is advantageous to operate the system at the highest possible pressure, thus optimizing system volumes for uncertainty and rise times.

### ***Two-Step Volume Measurement***

An example of the time history for the two-step measurement is shown in Figure C-5. The sample bottle (reference volume) is filled to the working pressure. Because of the unit design, the fuel stack is also subjected to this pressure for a short time, and some of the argon gas moves into the pellet stack. The sample bottle is then valved off, and the system, including the pellet stack, is pumped down to vacuum. Although it is difficult to see in Figure C-5, ~200 s are required to draw the gas out of the stack. For this step, the pellet stack is at the working pressure for only a short time (minutes not hours), thus limiting the amount of gas penetrating into the stack and presenting less of a pump-down challenge than if the system had been pumped down from an equilibrium high pressure in the stack.

To perform the two-step volume measurement, the sample bottle valve was opened, and the gas flowed into the plenum and fuel stack. It took ~150 s for the system to come to equilibrium at 167 psia (1.15 MPa). By comparing the pressure immediately after the valve opening with the pressure after the system reaches equilibrium, one might be able to estimate the plenum volume by using the instantaneous pressure, and the plenum-plus-pellet-stack volume might be estimated by using the equilibrium pressure, if the pressure sensor valve combination can respond fast enough.



**Figure C-4. Pressure history of a rod puncture.**

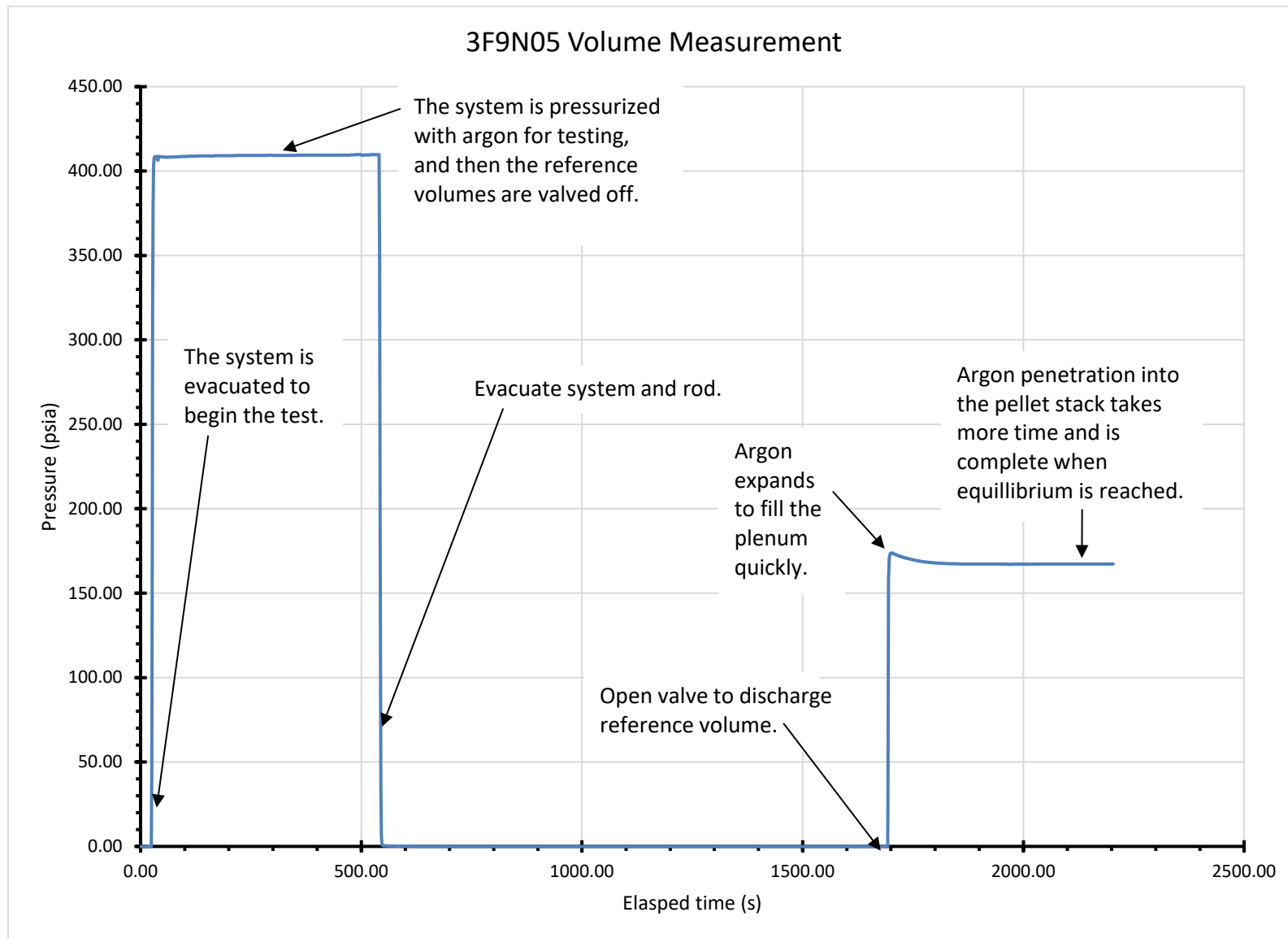


Figure C-5. Pressure history of a rod using the two-step method.

## C-4. Residual Gas Effects

### C-4.1 Estimated Time Required for Pumping out the Rod

The boundary conditions for pumping out the rod are different than the conditions for filling the rod, because the vacuum pump is essentially an infinite sink at zero pressure. In this case, it is assumed that the fuel rod is being pumped out through the plenum side so that the volume of interest is the pellet stack volume, and the starting pressure is essentially the rod pressure. Therefore, the equation developed for the rod transmission can be used, with the fixed pressure set equal to zero, as shown in Eq. (C-69) in Section C-5.

The equation starts with

$$\frac{dP_2}{dt} = \frac{KA}{2\mu LV_2} (P_1^2 - P_2^2), \quad (C-40)$$

where  $V_2$  is assumed to be the pellet stack volume, and  $P_2$  is assumed to be the stack pressure. Setting  $P_1$  equal to zero and dropping the subscripts gives

$$\frac{dP}{dt} = -\frac{KA}{2\mu LV} P^2, \quad (C-41)$$

and integrating gives

$$\frac{1}{P} = \frac{KA}{2\mu LV} t + \frac{1}{P_{rod}}. \quad (C-42)$$

Finally,

$$P = \frac{P_{rod}}{1 + \frac{P_{rod}KA}{2\mu LV} t}. \quad (C-43)$$

It is useful to estimate the time required to pump the rod down to 10% of the initial starting pressure:

$$\frac{10}{P_{rod}} - \frac{1}{P_{rod}} = \frac{KA}{2\mu LV} t, \quad (C-44)$$

$$t_{0.1} = \frac{18\mu LV}{KAP_{rod}}, \quad (C-45)$$

with:

$$A = 5 \times 10^{-5} \text{ m}^2,$$

$$\mu = 2.4 \times 10^{-5} \text{ Pa} \cdot \text{s},$$

$$L = 4 \text{ m},$$

$$V = V_{stack} = 2 \times 10^{-6} \text{ m}^3,$$

$$P_{rod} = 2.8 \times 10^6 \text{ Pa (lower pressure or fill for volume determination), and}$$

$$K = 2 \times 10^{-14} \text{ m}^2,$$

resulting in a time of about 1,200 s. This is once again a function of the rod pressure.

## C-4.2 Estimating the Volume of Gas that Could Be Trapped in the Pellet Stack following Rod Pump-Down

If the rod is pumped down and then switched into the both-chambers-sealed mode, then an estimate of the trapped gas can be obtained by monitoring the pressure increase using the primary equation for the gas flow (Section C-5):

$$\frac{dP_2}{dt} = \frac{KA}{2\mu LV_2} [P_1^2 - P_2^2]. \quad (C-46)$$

In this case,  $P_1$  is the gas in the stack, and  $P_2 \approx 0$ . This results in an equation that is applicable over short time periods:

$$\frac{dP_2}{dt} = \frac{KA}{2\mu LV_2} P_1^2. \quad (C-47)$$

Solving for the stack pressure,  $P_1$ , gives

$$P_1 = \sqrt{2 \frac{dP_2}{dt} \frac{\mu LV_2}{KA}}, \quad (C-48)$$

where typical parameters might be:

$$A = 5 \times 10^{-5} \text{ m}^2,$$

$$\mu = 2.4 \times 10^{-5} \text{ Pa} \cdot \text{s},$$

$$L = 4 \text{ M},$$

$$V_2 = V_{\text{apparatus}} + V_p = (25+9) \times 10^{-6} \text{ M}^3 = 34 \times 10^{-6} \text{ m}^3,$$

$$K = 2 \times 10^{-14} \text{ m}^2, \text{ and}$$

$$dP_2/dt = 0.01 \text{ psi in } 5 \text{ s} = 13.8 \text{ Pa/s},$$

resulting in about  $3 \times 10^5$  Pa, or 44 psia, for the trapped pellet stack pressure, which indicates the minimum pressure change that can be reliably detected with the gauge and setup. Thus, at low pressure, it might be difficult to determine when the pellet stack is truly pumped down because system outgassing or gauge limitations could mask this small measurement. The next section discusses how this situation can be mitigated by operating at high pressures with small volumes.

## C-4.3 Effects on Rod Void Volume Determination if Gas is Trapped in the Pellet Stack

The volume of the rod is often determined by evacuating it, backfilling it with a known volume at a known pressure, and then measuring the pressure of the combined system as detailed in the previous section:

$$P_{\text{fill}} V_{\text{ref}} = P_{\text{final}} (V_{\text{ref}} + V_{\text{rod}} + V_{\text{tare}}), \text{ giving} \quad (C-49)$$

$$\frac{P_{\text{fill}} V_{\text{ref}} - P_{\text{final}} (V_{\text{ref}} + V_{\text{tare}})}{P_{\text{final}}} = V_{\text{rod}}. \quad (C-50)$$

However, if some of the gas remains trapped in the pellet stack due to incomplete pump-down, then Eqs. (C-49) and (C-50) would become

$$P_{\text{fill}} V_{\text{ref}} + P_{\text{res}} V_{\text{stack}} = P_{\text{final}} (V_{\text{ref}} + V_{\text{rod}} + V_{\text{tare}}), \quad (C-51)$$

and

$$\frac{P_{fill}V_{ref} + P_{res}V_{stack} - P_{final}(V_{ref} + V_{tare})}{P_{final}} = V_{rod}, \quad (C-52)$$

where  $P_{res}$  is the unknown residual pressure left in the pellet stack, and  $V_{stack}$  is the volume of the pellet stack (a fraction of  $V_{rod}$ ). To estimate the impact of this residual pressure, its incremental effect can be examined by taking the derivative of Eq. (C-52):

$$\frac{\partial V_{rod}}{\partial P_{res}} = \frac{V_{stack}}{P_{final}} - \frac{(P_{fill}V_{ref} + P_{res}V_{stack} - P_{final}(V_{ref} + V_{tare}))}{P_{final}^2} \frac{\partial P_{final}}{\partial P_{res}}, \quad (C-53)$$

simplifying

$$\frac{\partial V_{rod}}{\partial P_{res}} = \frac{V_{stack}}{P_{final}} - \frac{V_{rod}}{P_{final}} \frac{\partial P_{final}}{\partial P_{res}}, \quad (C-54)$$

and next,

$$\frac{\partial P_{final}}{\partial P_{res}} = \frac{V_{stack}}{(V_{ref} + V_{rod} + V_{tare})} - \frac{(P_{fill}V_{ref} + P_{res}V_{stack})}{(V_{ref} + V_{rod} + V_{tare})^2} \frac{\partial V_{rod}}{\partial P_{res}}, \quad (C-55)$$

and simplifying

$$\frac{\partial P_{final}}{\partial P_{res}} = \frac{V_{stack}}{(V_{ref} + V_{rod} + V_{tare})} - \frac{P_{final}}{(V_{ref} + V_{rod} + V_{tare})} \frac{\partial V_{rod}}{\partial P_{res}}. \quad (C-56)$$

Equations (C-54) and (C-56) are combined:

$$\frac{\partial V_{rod}}{\partial P_{res}} = \frac{V_{stack}}{P_{final}} - \frac{V_{rod}}{P_{final}} \left[ \frac{V_{stack}}{(V_{ref} + V_{rod} + V_{tare})} - \frac{P_{final}}{(V_{ref} + V_{rod} + V_{tare})} \frac{\partial V_{rod}}{\partial P_{res}} \right]. \quad (C-57)$$

Simplifying further,

$$\frac{\partial V_{rod}}{\partial P_{res}} \left[ 1 - \frac{V_{rod}}{(V_{ref} + V_{rod} + V_{tare})} \right] = \frac{V_{stack}}{P_{final}} - \frac{V_{rod}V_{stack}}{P_{final}(V_{ref} + V_{rod} + V_{tare})} \quad (C-58)$$

$$\frac{\partial V_{rod}}{\partial P_{res}} \left[ 1 - \frac{V_{rod}}{(V_{ref} + V_{rod} + V_{tare})} \right] = \frac{V_{stack}}{P_{final}} \left[ 1 - \frac{V_{rod}}{(V_{ref} + V_{rod} + V_{tare})} \right], \quad (C-59)$$

and finally:

$$\frac{\partial V_{rod}}{\partial P_{res}} = \frac{V_{stack}}{P_{final}} = \frac{V_{stack}(V_{ref} + V_{rod} + V_{tare})}{(P_{fill}V_{ref} + P_{res}V_{stack})}. \quad (C-60)$$

Examining around  $P_{res} = 0$  gives

$$\Delta V_{rod} \approx \frac{V_{stack}(V_{ref} + V_{rod} + V_{tare})}{P_{fill}V_{ref}} \Delta P_{res}. \quad (C-61)$$

Thus, a small, unaccounted for residual pressure in the fuel stack results in an apparent increase in rod volume. Some typical values are as follows:

$$V_{stack} = 2 \text{ cc},$$

$$V_{ref} = 25 \text{ cc},$$

$$V_{tare} = 25 \text{ cc},$$

$$V_{rod} = 11 \text{ cc},$$

$$P_{fill} = 400 \text{ psia (2.76 MPa), and}$$

$$P_{res} = 40 \text{ psia (0.28 MPa) (assume 10% trapped gas in pellet stack).}$$

This gives 0.49 cc excess volume for an incompletely pumped down system. An incompletely pumped down system results in an apparent increase in volume, assuming that enough time has been allowed for the system to be close to equilibrium. For these values, the uncertainty from measurement, as discussed in previous sections, is about the same, so some target pump-down times, residual gas levels, and fill pressures can be seen. A large tare volume and a low fill pressure relative to the residual pressure exacerbate the situation. Also, comparing the two-step and double expansion methods provides some indication of the success of the methods, because a much larger two-step volume would cast doubt on the efficiency of the pump-down for its volume measurement.

#### C-4.4 Impact of Different Rod and Reference Volume Temperatures

To take the volume measurements, the fuel rod and tare volumes are pumped down to zero pressure, and the reference volume is filled to known pressure  $P_s$ . There could be a small difference between the hot cell and the operating area, so the temperature must be included when summing moles of gas. To perform the measurement, the valve is opened, as described in the previous sections, and the system is allowed to come to equilibrium (Figure C-6):

$$P_f \left( \frac{V_p}{T_p} + \frac{V_t}{T_t} + \frac{V_r}{T_r} \right) = \frac{P_s V_r}{T_r}. \quad (\text{C-62})$$

Thus,

$$\frac{V_p}{T_p} = \frac{P_s V_r}{P_f T_r} - \left( \frac{V_t}{T_t} + \frac{V_r}{T_r} \right). \quad (\text{C-63})$$

The case of interest is when  $T_p$  and  $T_t$  are about the same and are somewhat different from  $T_r$ . Thus:

$$V_p = T_p \left[ \frac{P_s V_r}{P_f T_r} - \left( \frac{V_t}{T_t} + \frac{V_r}{T_r} \right) \right] = \frac{T_p P_s V_r}{P_f T_r} - V_t - \frac{T_p V_r}{T_r} = \frac{T_p}{T_r} \left[ \frac{P_s V_r}{P_f} - V_r \right] - V_t. \quad (\text{C-64})$$

Note that  $V_r$  is effectively increased by the temperature ratio:

$$V_p = V_r \frac{T_p}{T_r} \left[ \frac{P_s}{P_f} - 1 \right] - V_t. \quad (\text{C-65})$$

Therefore, a first approximation correction to the temperature difference is to multiply the reference volume by the temperature ratio. A small temperature gradient will exist along the lines that connect the in-cell equipment to the out-cell equipment, but the volume of these lines is small compared with the other volumes.

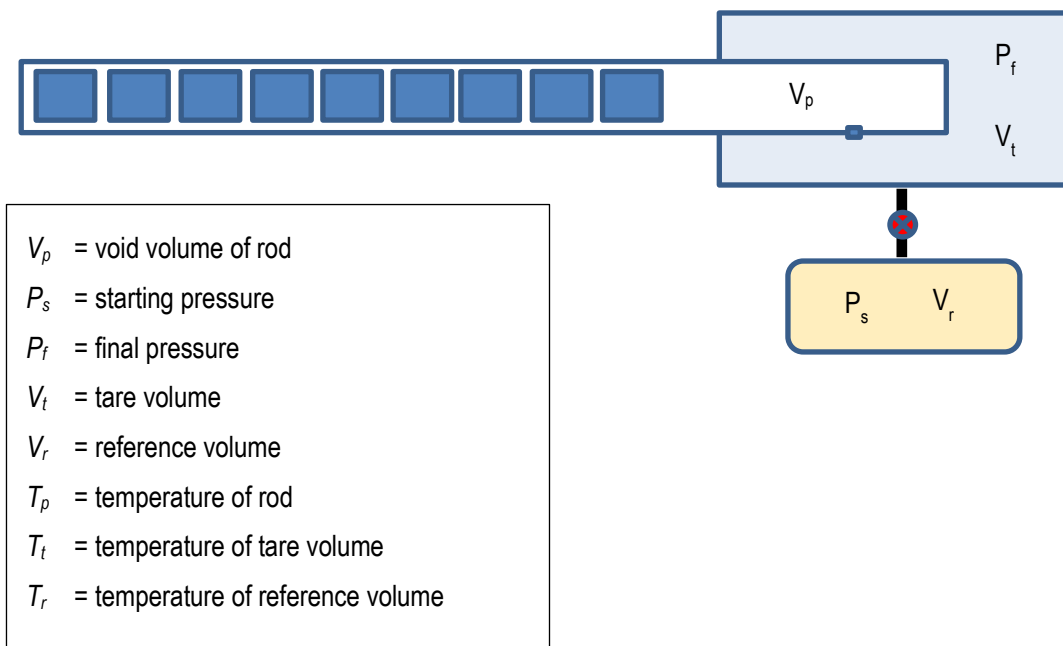


**Figure C-6. System used to estimate the effects of small temperature differences between the fuel rod in the hot cell and the test control apparatus on the outside.**

## C-5. Depressurization and Gas Transmission Test Operation and Design Considerations

The typical design of pressurized water reactor (PWR) fuel rods includes a small gap between the pellet OD and the cladding ID, as well as a plenum volume at the top of the fuel rod that provides void volume for the helium gas used to pre-pressurize the rods. In addition to the gap and plenum void volumes, the sister rods' pellets include chamfers and dishes, and those void volumes provide a relatively large reservoir throughout the pellet stack for pre-pressurization gas. At beginning of life, these relatively large void volumes provide an open pathway for gas transmission up to the onset of pellet-cladding interaction (PCI). By the end of the first cycle, cladding creep-down and pellet swelling tend to close the gap between the pellet OD and the cladding ID, and after PCI, gas transmission is restricted because the gap is no longer open. The amount of PCI varies axially. Local fission gas production and its release to the rod void volume are variable along the axial length of the rod because power, fluence, and fuel temperature vary radially and axially within the fuel rod.

However, as the rod is operated in the reactor, additional circulation paths through the pellet stack are developed, depending on local operating conditions. The process is somewhat stochastic and is related to thermal cycling of the fuel, crack development in the pellet due to thermal stresses, and crack self-healing. Once the fuel is discharged, the flow path becomes essentially fixed [C-4, C-5].

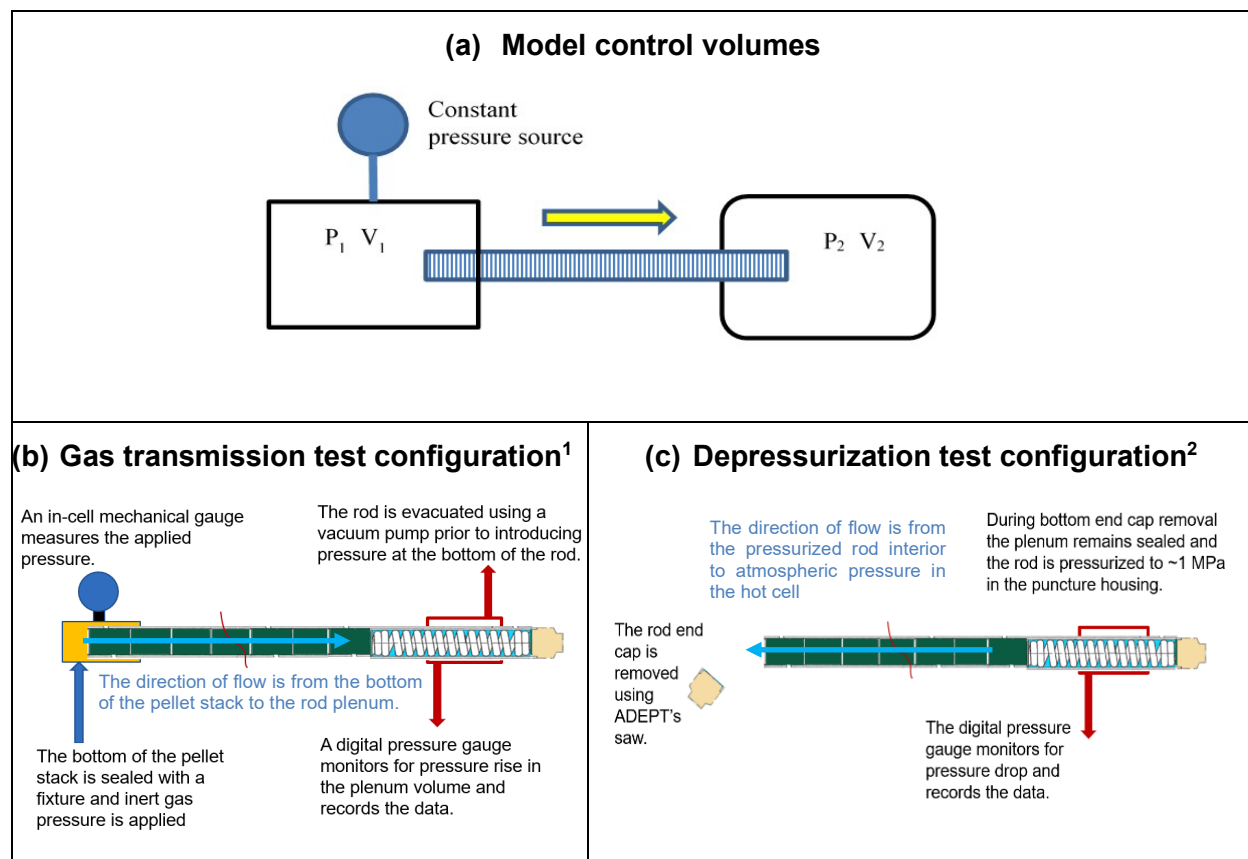
Gas transmission tests were performed to characterize the ability for helium and fission gases to move through the pellet stack. All punctured sister rods were subjected to a depressurization test, and three sister rods were also subjected to a gas transmission test. For the depressurization test, after the rod internal pressure and void volume measurements were complete, the rod's bottom endcap was cut off. Pressurized argon (~175 psia [1.21 Mpa] remained in the rod following the final two-step volume measurement) flowed from the plenum through the pellet stack and out through the bottom of the rod to atmospheric pressure, and the pressure drop with time at the plenum was recorded. This depressurization measurement provided an initial indication of the resistance to fission gas transmissibility within the pellet stack and demonstrated gas communication from one side of the stack to the other at room temperature. For the gas transmission test, the free rod volume was evacuated, and a constant pressure source was connected at the open bottom of the rod. The gas flowed from the lower end of the rod along the pellet stack to the plenum, and the pressure rise with time was recorded. Two or three different tests were completed for three rods at different pressures.

The movement of gas through a fuel rod pellet stack can be modeled as a pressure source connected to one end of the fuel rod and a pressure-monitored fixed volume reservoir connected at the other end with both ends open to the fuel stack, as shown in Figure C-7. At the start of the gas transmission test, the reservoir end is at near zero pressure, and the source is essentially at a fixed pressure for the duration of the test (Figure C-7[b]). For the depressurization test, the reservoir end starts at a positive pressure, while the other end is at atmospheric pressure, and the reservoir is slowly discharged (Figure C-7[c])

Following the measurement of the rod's internal pressure and void volume, the rod is left sealed in the puncture housing. The rod is typically at ~170 psia (1.17 MPa) with argon after this test, and V1, V3, and V4 are closed (V4 had been open for an earlier test). The bottom end of the rod is then clamped in place, and the ADEPT saw is used to cut off the end of the rod approximately 5 mm above the endcap weld. The time vs. pressure is recorded until the pressure measured is near equilibrium. The endcap that was cut off is saved in a labeled container.

Following depressurization testing, a support is placed over the open bottom end of the fuel rod and clamped in place (Figure C-8). The support includes a pressurizing unit with a large mechanical gauge that can be monitored through the hot cell window. A brace is placed at the top end of the rod to prevent any axial motion as the rod is pressurized (Figure C-9).





<sup>1</sup> After the end of the rod is cut off and depressurization of the rod is complete, a compression fitting is sealed over the cut end, and pressurized gas is introduced.

<sup>2</sup> The plenum end of the fuel rod is pressurized with an inert gas. The end of the rod is removed, providing an outlet at atmospheric pressure.

**Figure C-7. Schematics of the depressurization and gas transmission test configurations.**

Valves V1, V2, and V5 are opened to pump the system down, and the pressure to the support is turned on and adjusted. Valves V1, V2, and V5 are then closed. The pressure at the source end is monitored manually by viewing the mechanical gauge. The pressure in the rod plenum is recorded with time using the digital gauge until an equilibrium has been reached or until essentially full pressure is obtained.

Schematics of the model control volumes and depressurization and gas transmission configurations are shown in Figure C-7(a)–(c). The depressurization test and the gas transmission test are constructed with a constant pressure source connected to one end of the fuel rod and a pressure-monitored fixed volume reservoir connected at the other end; both ends are open to the pellet stack as shown in Figure C-7(b) or Figure C-7(c), with the flow in opposite directions for the two configurations. The fuel rod system is divided into two control volumes connected by a flow path composed of the rod pellet stack with the control volumes and pressures, as illustrated in Figure C-7(a).

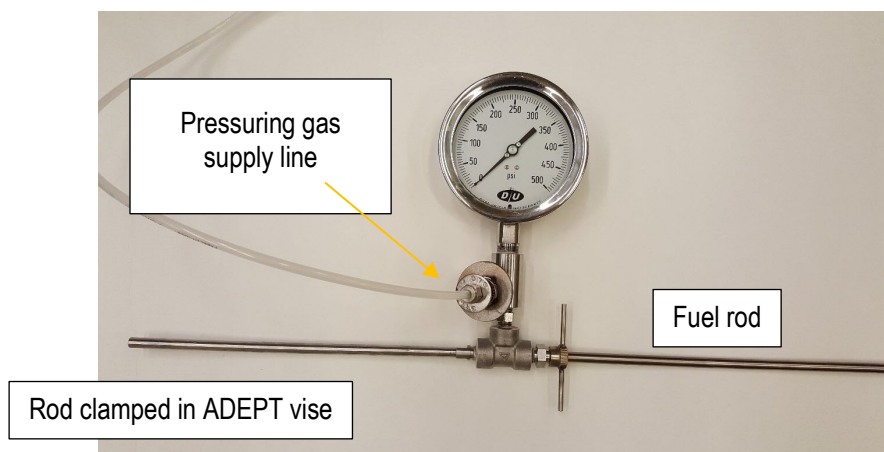


**Figure C-8. Rod inserted into the gas transmission support fixture with the pressure gauge and pressure supply line.**

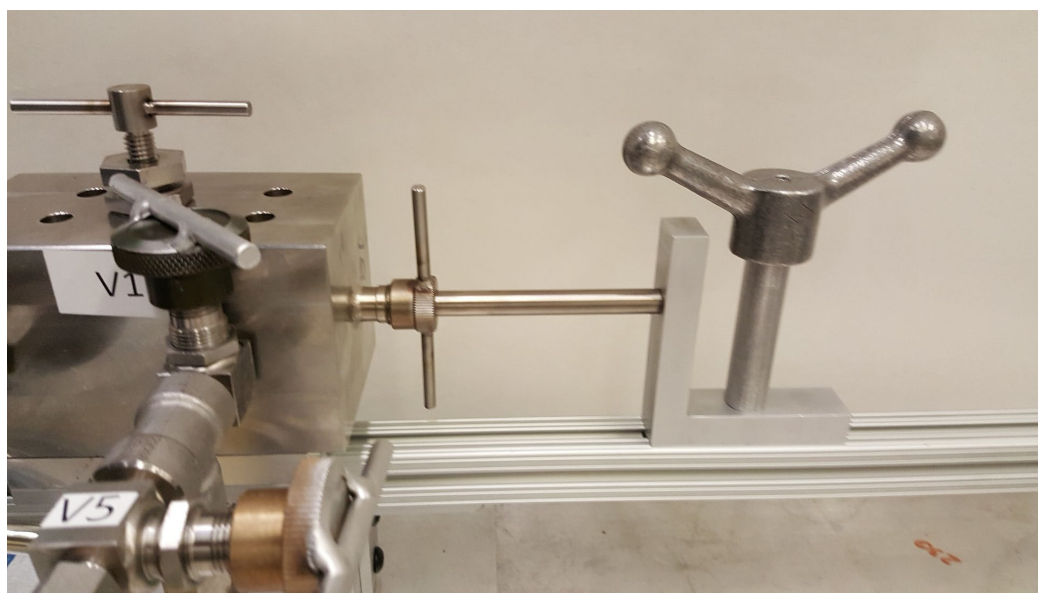


**Figure C-9. Plenum end support brace in place to prevent the rod from moving forward.**

To describe the average gas transmissibility through the complete pellet stack and quantify a permeability coefficient, the pellet stack is modeled as a single unit. The stack is considered a 1D flow path that has closely packed coarse irregular media (e.g., cracked  $\text{UO}_2$  pellets) with a pressure differential across the media. The flow conditions are assumed to be isothermal.

To describe the movement of fission gas through the pellet stack, Muskat's porous media flow application of Poiseuille's equation (i.e., compressible flow through a long cylindrical pipe) is used to approximate the flow to allow for comparison with previous work on this topic [C-6–C-9].

For the depressurization test, the plenum region pressure ( $P_2$ ) starts at a high pressure and decays through the pellet stack, and the rod's bottom end pressure ( $P_1$ ) is held constant at atmospheric pressure. This test is conducted by cutting off the bottom of the rod just after the rod plenum volume measurement is taken, as illustrated in Figure C-7(c). Before the depressurization test, the rod is evacuated and backfilled with

the test gas. For the gas transmission test, a constant test gas pressure ( $P_1$ ) is applied to the cutoff rod end while the pressure ( $P_2$ ) in the plenum volume ( $V_2$ ) is measured after first being evacuated, as shown in Figure C-7(b).

All tests were performed in the hot cell at room temperature using argon as the test gas because it is closer in molecular weight to the fission gases. The heavier weight gases are more likely to be trapped or impeded by tortuosity within the pellet stack flow paths, unlike helium, which moves through most materials very quickly. Although xenon would have been the best gas to use, it is very expensive and difficult to obtain in large quantities. Table C-2 specifies the material properties and the rods' physical dimensions used in the calculations.

**Table C-2. Argon material properties used in calculations.**

Parameter	Value
Dynamic gas viscosity of argon	2.42E-05 Pa-s
Stack length (typical)	3.65 m
Area cross section	5.15E-05 m <sup>2</sup>
Measuring volume (rod plenum plus tare, typical)	3.77E-05 m <sup>3</sup>

## C-5.1 Data Analysis and Fitting

The flow through the fuel rod is modeled as Muskat's application of Poiseuille flow through a porous media. This pressure-driving force is related to the difference between the squares of the two volumes' pressures; the steady-state mass flow solution for two connected reservoirs at different pressures, and constant temperatures through a flow impedance is (constant pressure, steady state conditions) [C-10]:

$$\frac{dm_2}{dt} = \frac{KAM}{2\mu LRT} (P_1^2 - P_2^2), \quad (C-66)$$

where

- $dm_2/dt$  is the mass flow rate into  $V_2$  (Kg/s);
- $K$  is the permeability coefficient (m<sup>2</sup>) for a homogenous medium;
- $A$  is the cross sectional flow area of the flow (m<sup>2</sup>), in this application, the cross-sectional area of the space inside the fuel rod where the bulk flow is along the longitudinal axis of the rod;
- $M$  is the molecular mass of the gas (Kg/mol);
- $L$  is the length over which pressure drop occurs (m), in this application, the pellet stack length;
- $\mu$  is the dynamic viscosity (Pa·s);
- $P_i$  is the pressure in volume  $i$  (Pa);
- $R$  is the gas constant; and
- $T$  is the temperature.

From the ideal gas law for Volume 2,

$$n_2 = \frac{m_2}{M} = \frac{P_2 V_2}{RT}. \quad (C-67)$$

Taking the derivative of Eq. (C-67) gives

$$\frac{dm_2}{dt} = \frac{MV_2}{RT} \frac{dP_2}{dt}. \quad (C-68)$$

Combining Eqs. (C-66) and (C-68) gives

$$\frac{dP_2}{dt} = \frac{KA}{2\mu LV_2} (P_1^2 - P_2^2). \quad (C-69)$$

This can be integrated to give ( $P_1 \neq 0$ )

$$\frac{P_1 - P_2}{P_1 + P_2} = P_{0p} e^{-K\eta t}, \quad (C-70)$$

where  $P_{0p}$  is a constant of integration and  $\eta = \frac{P_1 A}{V_2 \mu L}$ . At  $t=0$ ,

$$\frac{P_1 - P_2(t=0)}{P_1 + P_2(t=0)} = P_{0p}. \quad (C-71)$$

Finally,

$$P_2 = \frac{P_1(1 - P_{0p} e^{-K\eta t})}{(1 + P_{0p} e^{-K\eta t})}. \quad (C-72)$$

The Darcy solution (i.e., linear pressure differential) is mentioned for comparison with incompressible flow conditions. A derivation similar to that provided here for the Muskat-Poiseuille application can also be performed but is not included here. Darcy's law provides a simple proportional relationship between the fluid flow rate and the pressure drop for an incompressible flow through a porous medium. In the case of the HBU fuel rod geometry, Darcy's law is

$$Q = -\frac{K A (P_1 - P_2)}{\mu L}, \quad (C-73)$$

where

$Q$  is volumetric flow rate ( $m^3$ ) or  $dV/dt$ ;

$K$  is permeability ( $m^2$ ) of a homogenous porous medium;

$A$  is the cross-sectional flow area of the flow ( $m^2$ ), in this application, the cross-sectional area of the space inside the fuel rod where the bulk flow is along the longitudinal axis of the rod;

$L$  is the length over which the pressure drop occurs (m), in this application, the pellet stack length;

$\mu$  is dynamic viscosity ( $Pa \cdot s$ );

$P_1$  is pressure (Pa) in volume V1 (Figure C-7); and

$P_2$  is pressure (Pa) in volume V2 (Figure C-7).

Because Darcy's law is only valid for single-phase incompressible laminar flows, it is not expected to produce a good fit for the HBU fuel rods. Darcy's law solution is provided here for comparison.

The Darcy's law solution to evaluate the permeability from the data is [C-6,C-7]

$$P_2 = P_1 - (P_1 - P_2(t=0))e^{-K\eta t}. \quad (C-74)$$

## C-5.2 Application to Sealed Rods

Most fuel rods are expected to be sealed during transport. If road vibrations cause additional pellet cracking or pellet clad debonding, which releases gas trapped in sealed voids or pores, then the rod will no longer be at a constant equilibrium pressure, and gas will move from one end of the rod to another. This section presents a further examination of the expected response given the proposed model.

If both end chambers are sealed, then the volumes are constant with time, and the total system moles do not change, even though the pressure can, thus resulting in (for constant temperature):

$$V_1 P_1 + V_2 P_2 = \mathbb{Z}. \quad (C-75)$$

March 31, 2022

This can be inserted into Eq. (C-69):

$$\frac{dP_2}{dt} = \frac{KA}{2\mu LV_2} \left[ \left( \frac{\mathbb{Z} - V_2 P_2}{V_1} \right)^2 - P_2^2 \right] = \frac{KA(V_2^2 - V_1^2)}{2\mu LV_1^2 V_2} \left[ P_2^2 - \frac{2\mathbb{Z}V_2 P_2}{(V_2^2 - V_1^2)} + \frac{\mathbb{Z}^2}{(V_2^2 - V_1^2)} \right]. \quad (C-76)$$

Factoring gives

$$\frac{dP_2}{dt} = \frac{KA(V_2^2 - V_1^2)}{2\mu LV_1^2 V_2} \left[ P_2 - \frac{\mathbb{Z}(V_2 + V_1)}{(V_2^2 - V_1^2)} \right] \left[ P_2 - \frac{\mathbb{Z}(V_2 - V_1)}{(V_2^2 - V_1^2)} \right], \quad (C-77)$$

or

$$\frac{dP_2}{\left[ P_2 - \frac{\mathbb{Z}(V_2 + V_1)}{(V_2^2 - V_1^2)} \right] \left[ P_2 - \frac{\mathbb{Z}(V_2 - V_1)}{(V_2^2 - V_1^2)} \right]} = \frac{KA(V_2^2 - V_1^2)}{2\mu LV_1^2 V_2} dt. \quad (C-78)$$

Put into a form for integration,

$$\left\{ \frac{1}{\left[ P_2 - \frac{\mathbb{Z}(V_2 + V_1)}{(V_2^2 - V_1^2)} \right]} - \frac{1}{\left[ P_2 - \frac{\mathbb{Z}(V_2 - V_1)}{(V_2^2 - V_1^2)} \right]} \right\} dP_2 = \frac{\mathbb{Z}KA}{\mu LV_1 V_2} dt. \quad (C-79)$$

Integrating gives

$$\ln \left[ P_2 - \frac{\mathbb{Z}(V_2 + V_1)}{(V_2^2 - V_1^2)} \right] - \ln \left[ P_2 - \frac{\mathbb{Z}(V_2 - V_1)}{(V_2^2 - V_1^2)} \right] = \frac{\mathbb{Z}KA}{\mu LV_1 V_2} t - \ln(-P_0), \quad (C-80)$$

where  $P_0$  is a constant of integration. Finally,

$$\frac{\left[ \frac{\mathbb{Z}(V_2 - V_1)}{(V_2^2 - V_1^2)} - P_2 \right]}{\left[ \frac{\mathbb{Z}(V_2 + V_1)}{(V_2^2 - V_1^2)} + P_2 \right]} = P_0 e^{-K\omega t}, \quad (C-81)$$

with

$$\omega = \frac{\mathbb{Z}A}{\mu LV_1 V_2}. \quad (C-82)$$

Solving for  $P_2$ ,

$$P_2 = \frac{\mathbb{Z}}{(V_2^2 - V_1^2)} \frac{[(V_2 - V_1) + (V_2 + V_1)P_0 e^{-K\omega t}]}{[1 + P_0 e^{-K\omega t}]}. \quad (C-83)$$

For  $V_1 \rightarrow \infty$ ,  $\omega \rightarrow \eta$  as expected, and Eq. (C-72) is recreated.  $P_0$  can be determined from Eq. (C-83) at  $t=0$ .

The case of most interest for the puncture application is when  $P_1$  is the rod pressure,  $P_2$  is the vacuum of a puncture unit,  $V_1$  is the volume of the pellet stack, and  $V_2$  is the volume of the rod plenum and puncture unit. This is the approximate situation in which a fuel rod is being punctured or a volume measurement is being taken. In this case, a zero-dimensional approximation can be made for the starting condition by assuming that the rod's pressure and pellet stack interstitial volume is at the bottom of the rod, the pellets form the impedance path, the top plenum is punctured and instantly connected to the puncture apparatus, and the combined volume of the apparatus and plenum is at the now-expanded plenum pressure. The goal is to compute the approximate equilibrium time for the pellet stack to come to equilibrium with the plenum plus the apparatus pressure. Thus,

$$\mathbb{Z} = P_{rod} V_{stack} + P_{pun}(V_{apparatus} + V_p). \quad (C-84)$$

It is useful to estimate the time constant for parameters of interest:

$$A = 5 \times 10^{-5} \text{ M}^2$$

$$\mu = 2.4 \times 10^{-5} \text{ Pa} \cdot \text{s}$$

$$L = 4 \text{ M}$$

$$V_1 = V_{\text{stack}} = 2 \times 10^{-6} \text{ M}^3$$

$$V_2 = V_{\text{apparatus}} + V_p = (25+9) \times 10^{-6} \text{ M}^3 = 34 \times 10^{-6} \text{ M}^3$$

$$P_{\text{rod}} = 4 \times 10^6 \text{ Pa}$$

$$P_{\text{pun}} = 1.06 \times 10^6 \text{ Pa}$$

$$Z = V_1 \times P_{\text{rod}} + V_2 \times P_{\text{pun}} = 2 \times 10^{-6} \text{ M}^3 \times 4 \times 10^6 \text{ Pa} + 34 \times 10^{-6} \text{ M}^3 \times 1.06 \times 10^6 \text{ Pa} = 44 \text{ M}^3 \cdot \text{Pa}$$

$$K = 2 \times 10^{-14} \text{ M}^2$$

The time constant for a case in which all the stack volume is at the very end of the rod, away from the puncture point (it might be more reasonable to use half the rod length), is:

$$T_c = \frac{\mu L V_1 V_2}{K A Z}, \quad (\text{C-85})$$

or about 150 s, or ~2.5 min for what might be considered the worst case; using half the rod length for the estimate gives half the time. Low system pressures and large apparatus volumes take much longer. Thus, one goal is to take rod measurements by using the highest practical pressures and the smallest apparatus volumes.

## C-6. Rod Internal Pressure and Void Volume Measurements of the Sister Rods

The gas pressure and void volume of a fuel rod was measured by puncturing the plenum region of the rod and using the ideal gas law in conjunction with known pressures and volumes. The plenum end of the fuel rod was sealed into an evacuated housing of known volume (the *tare* volume). After puncture, the pressure in the housing was measured, and then the gas was expanded into another chamber of known volume, and the new pressure was measured. This double expansion method allowed the rod's internal pressure and free internal volume to be determined. Once measurements were completed, the housing and the now-accessible free rod volume were evacuated and backfilled with a known volume and pressure of gas, and the final gas pressure was measured. This process allowed a second two-step measurement of the rod's void volume and a second calculation for the rod's internal pressure.

The results of the rod internal pressure and void volume measurements for the 8 sister rods punctured to date are shown in Table C-3, along with the  $2\sigma$  uncertainty. The double expansion method measured both volume and rod pressure in a single action and had a somewhat higher uncertainty than the two-step method, which measured the volume separately from the pressure measurement and thus offered a small improvement in uncertainty. Rod 30AK09 had a faulty measurement in the second expansion operation, so the double expansion results were invalid; however, the two-step method provided usable results. The rod puncture left a very small hole in the plenum region of the rod, estimated to be less than  $\frac{1}{2}$  mm in diameter.

### C-6.1 Comparisons of the Sister Rod Measured Internal Pressure and Void Volume with Available Data from Other Fuel Rods

Figure C-10 plots the sister rod's measured internal pressures with other PWR fuel rod data from the Electric Power Research Institute (EPRI) [C-11] and the sister rod internal pressure is within the envelope of the available information. Likewise, Figure C-11 plots the sister rod measured void volume with available EPRI data [C-11], demonstrating that the sister rod measured void volumes are within the extents of past measurements. However, while these general comparisons provide information about the sister rods relative to other commercial power PWR rods, direct comparisons cannot be made with the majority of the EPRI data because the mechanical design of the fuel rods are too diverse. Only four of the EPRI datapoints are from other  $17\times 17$  rods having a similar rod pre-pressurization of  $\sim 1.7\text{--}2.5$  MPa and are more directly comparable, although they were not operated in domestic reactors under the same conditions as the sister rods. Other array types within the EPRI data cited are not directly comparable, as design parameters such as initial design void volume, pellet density and grain size, initial fill pressure, and cladding alloy (in addition to the fuel operating temperature in reactor) can strongly influence the end-of-life internal pressure and void volume. Figure C-10 also includes four datapoints for Westinghouse  $17\times 17$  rods that were fabricated with an integral fuel burnable absorber (IFBA) coating on the fuel pellets [C-12]. The coating is typically a thin layer of zirconium diboride on the ODs of the pellets that is used for reactor reactivity control during reactor operation. None of the sister rods had IFBA coatings, but otherwise, the Westinghouse rods are very similar to the sister rods. It should be mentioned that the heat-treated Zirc-4-clad sister rod, F35P17, is expected to be atypical because it was operated to HBU for four cycles as a lead test rod and is at a higher burnup than other sister rods and the four comparable EPRI rods that were measured.

Plotting the partial pressure of the fission gas (the measured rod internal pressure minus the rod design pre-pressurization [as adjusted for the change in void volume]) with rod average burnup yields similar information, as shown in Figure C-12. Note that the initial void volume is not available for the EPRI data, and the fission gas partial pressures for those reference datapoints were calculated assuming a volume adjustment of 1.2.

**Table C-3. Results of rod internal pressure and void volume measurements at 25°C.**

	cladding	Rod average burnup (GWd/MTU)	Pre-pressurization (MPa)	Measured pressure, double expansion (MPa) <sup>a</sup>	2 $\sigma$ (95% confidence interval) uncertainty <sup>a</sup>	Measured pressure, two-step (MPa)	2 $\sigma$ (95% confidence interval) Uncertainty	Volume (cc)	2 $\sigma$ (95% confidence interval) uncertainty
30AK09	M5	53	1.7	N/A <sup>b</sup>	N/A <sup>b</sup>	3.46	2.5%	9.89	4.0%
30AD05	M5	54	1.7	3.50	4.1%	3.46	2.7%	10.63	3.7%
30AE14 <sup>c</sup>	M5	54	1.7	3.25	4.0%	3.22	2.6%	10.99	3.6%
3D8E14	ZIRLO	59	2.0	4.14	3.0%	4.18	2.4%	11.73	3.4%
3F9N05 <sup>c</sup>	ZIRLO	54	2.0	4.02	2.9%	3.98	2.2%	12.74	3.2%
6U3K09	ZIRLO	55	2.0	3.74	3.5%	3.64	2.5%	11.78	3.5%
3A1F05	LT Zirc-4	51	2.0	3.73	2.9%	3.73	2.2%	12.94	3.2%
F35P17 <sup>c</sup>	Zirc-4	60	2.5	4.83	5.7%	4.68	3.8%	13.32	4.8%

<sup>a</sup> The double expansion method has a slightly higher uncertainty. The results are provided here as an independent measurement for information; however, the two-step method result is the cited result for the rod internal pressure and void volume measurements.

<sup>b</sup> A problem with the second expansion operation introduced an irrecoverable error to the double expansion measurement for this rod.

<sup>c</sup> The rod was heat treated as described in Appendix A.



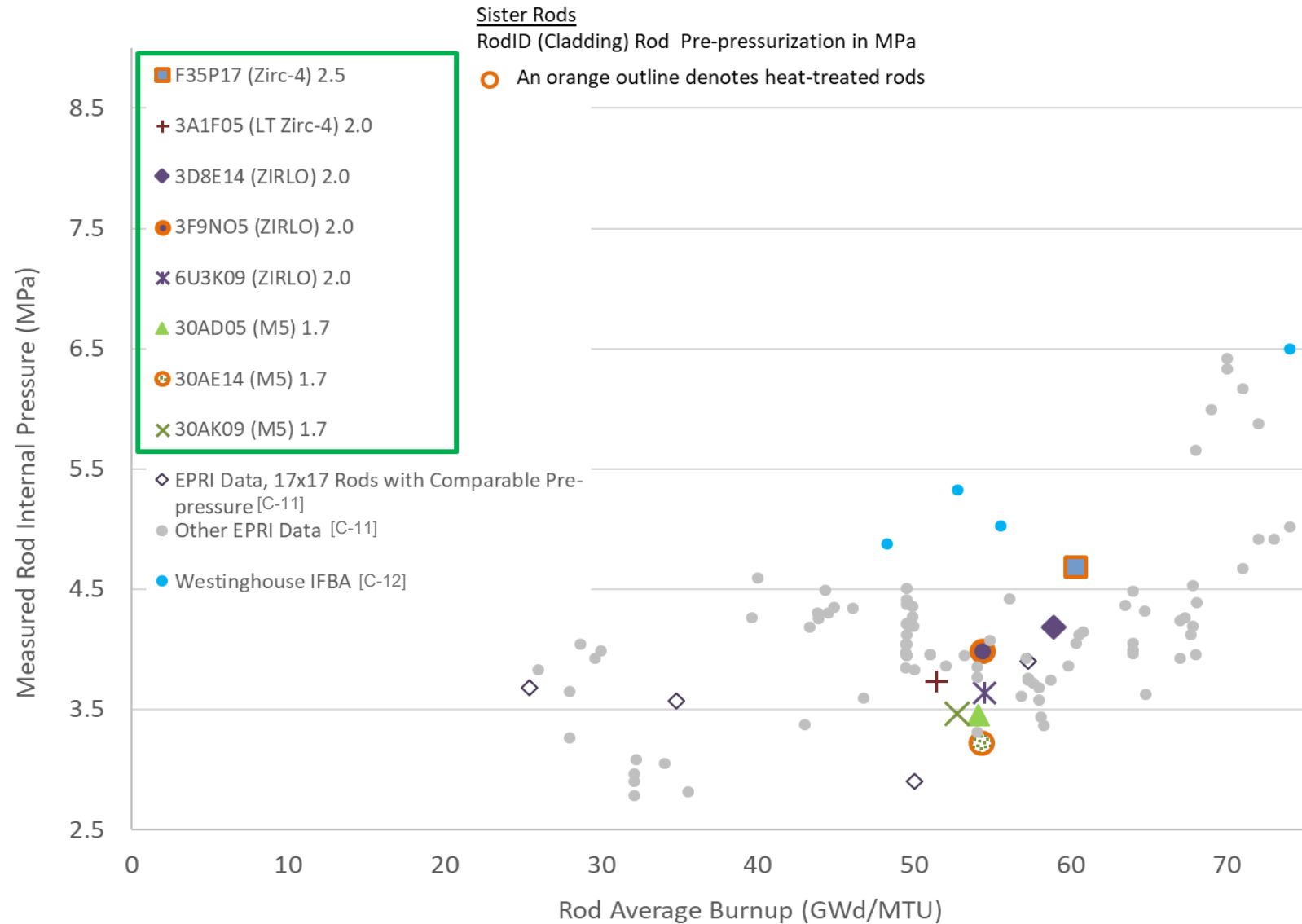


Figure C-10. Sister rod measured rod internal pressure at 25°C.

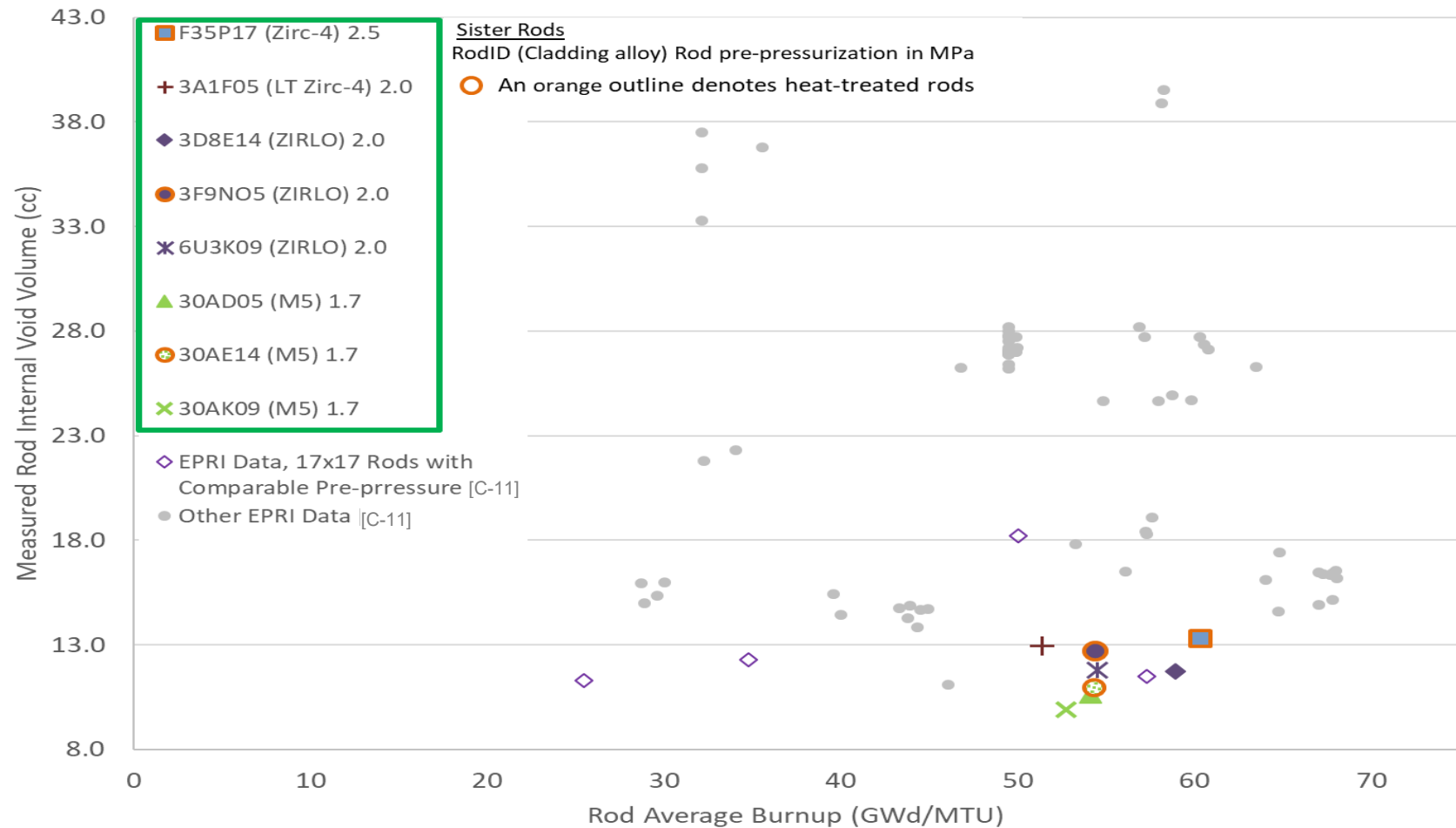


Figure C-11. Sister rod measured void volume 25°C with comparable historical data.

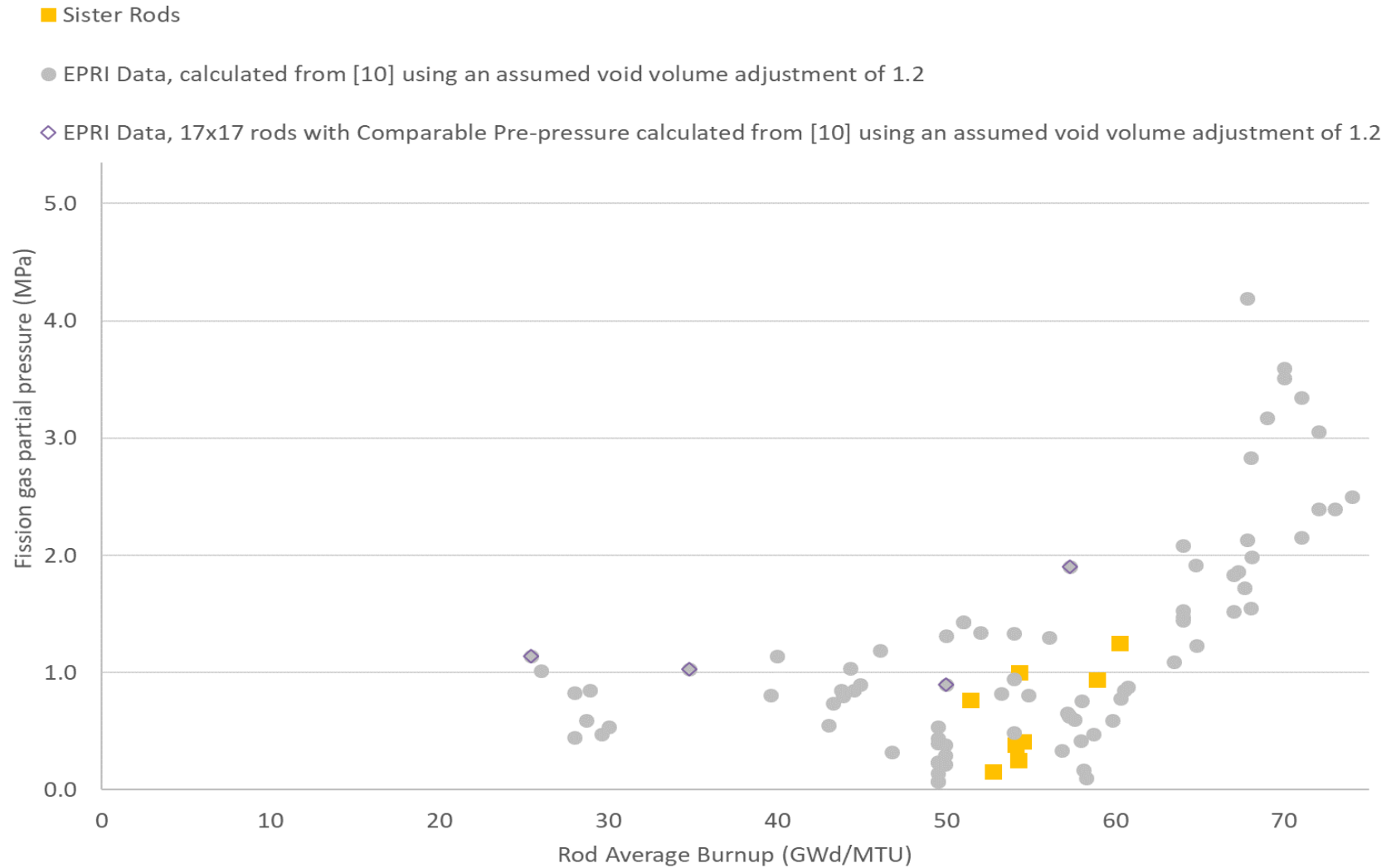


Figure C-12. Sister rod measured fission gas partial pressure at 25°C.

## C-6.2 Comparisons of the Measured Internal Pressure and Void Volume with Available Data from Other Sister Rods

Figure C-13a plots the measured rod internal pressure against the measured rod void volume and illustrates the expected grouping by vendor design/cladding type. For example, the Framatome-designed rods are consistent with each other, and the Westinghouse ZIRLO rods are consistent with each other. Figure C-13b plots the measured rod internal pressure as a function of the rod nominal design pre-pressure. A strong correlation is seen between the end-of-life and beginning-of-life pressures ( $R^2 > 0.6$ ).

Plots of the rod internal pressure with other parameters of interest such as the rod average burnup, assembly duty, average fuel temperature, and maximum fuel temperature (Figure C-14) indicate that these parameters are not as strongly correlated ( $0.4 < R^2 < 0.6$ ). This is likely due to the lack of a variety of data points within those parameters—as the range of burnup is small—combined with measurement uncertainties and inaccuracies in the rod's design and operational data (e.g., the maximum assembly middle-of-cycle temperature reported may not correspond to the sister rod's operating location). When considering only the fission gas partial pressure, the design and operational data are correlated at about the same quality ( $R^2 \approx 0.4$ ), as shown in Figure C-15. More data for rods at other operating conditions are required to further evaluate the measured pressure and volume data within the context of power operation.

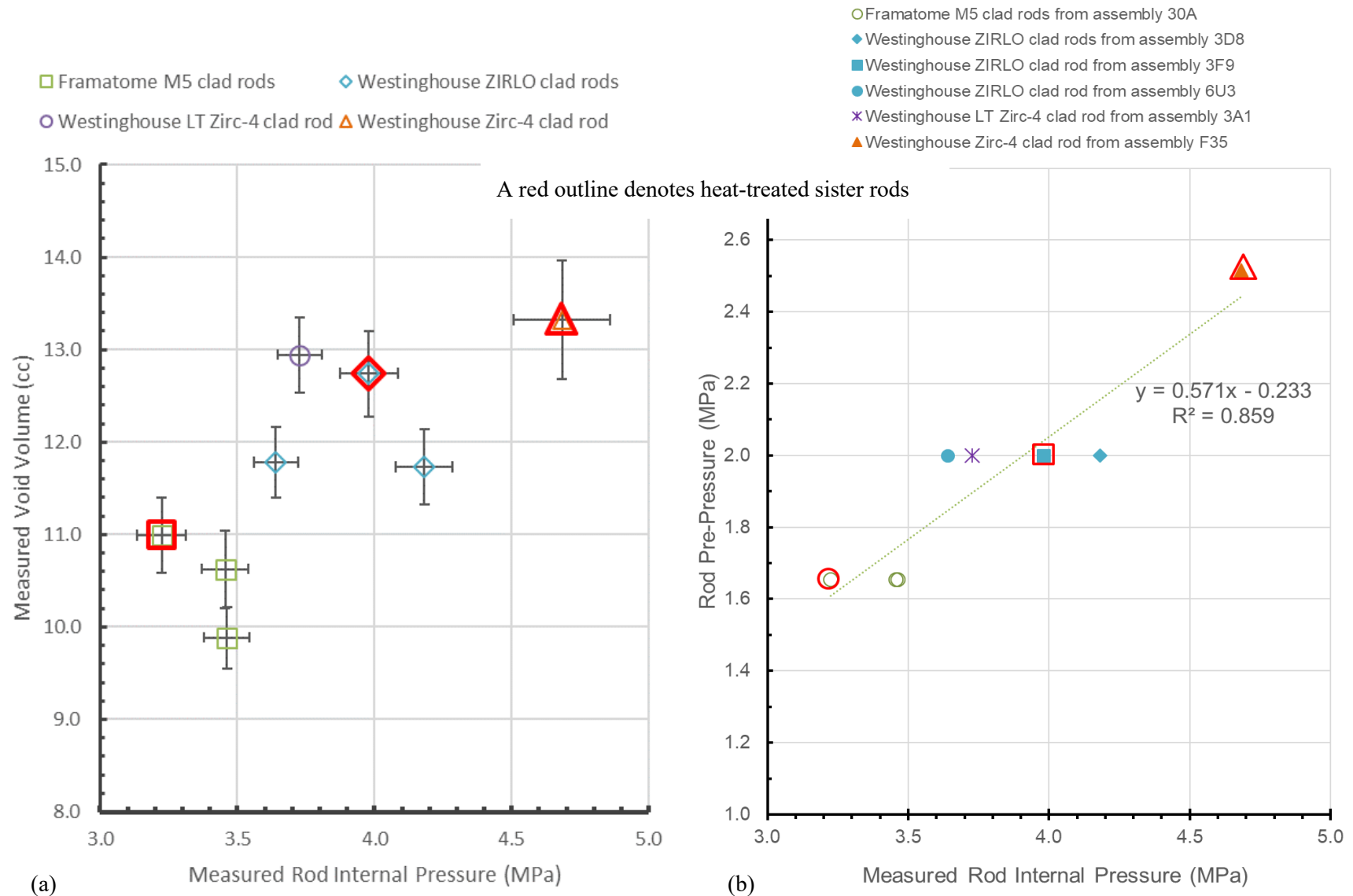
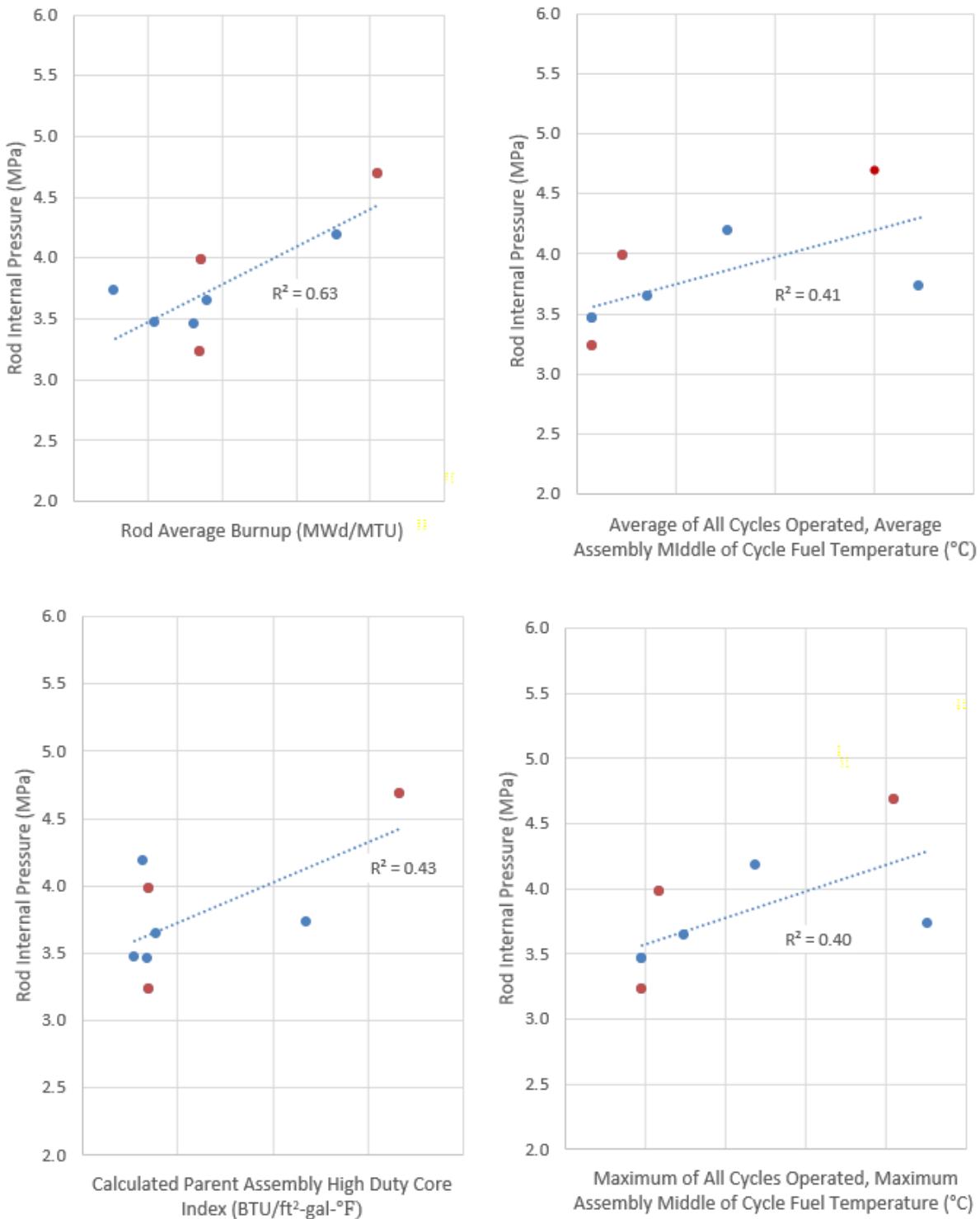
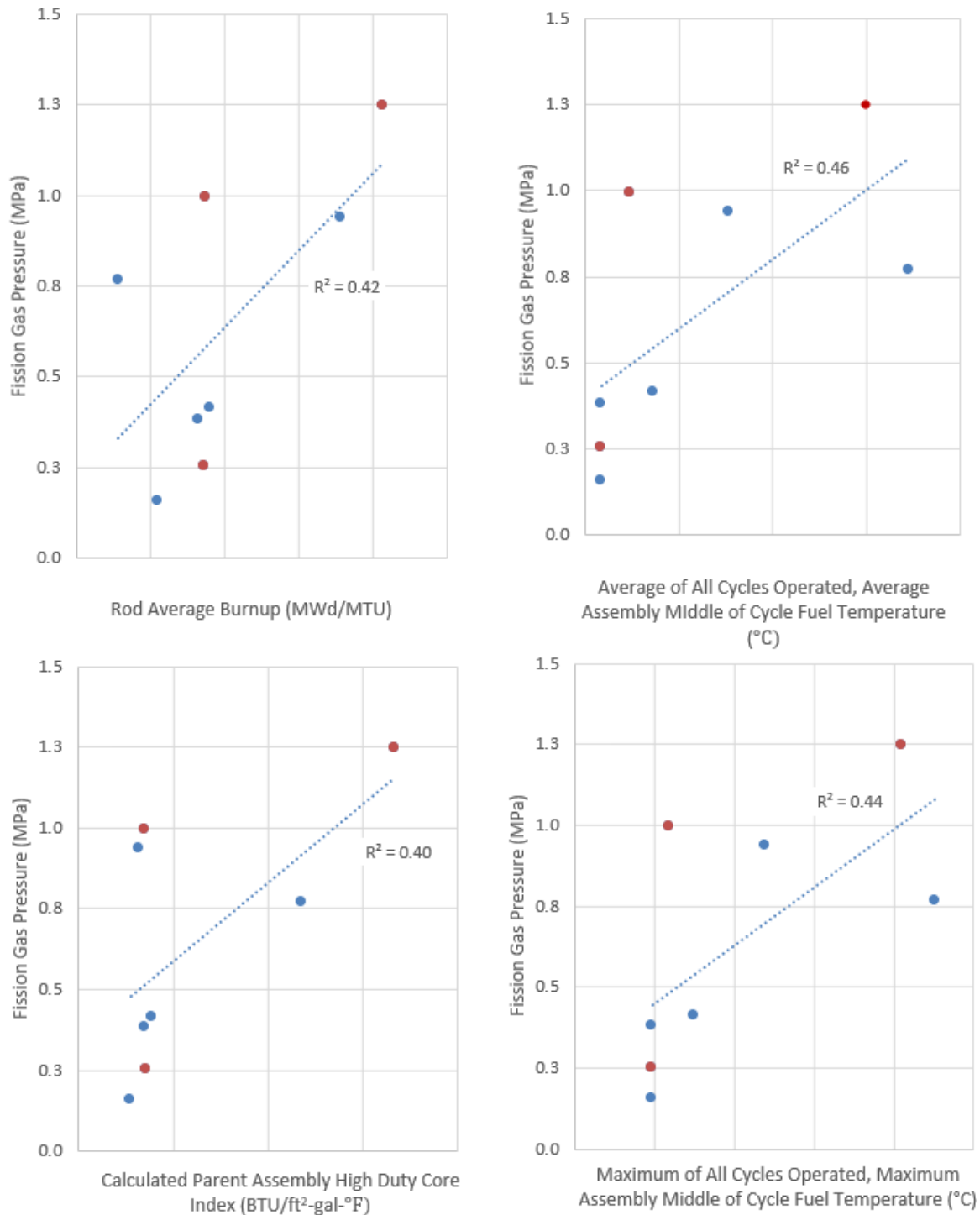


Figure C-13. Sister rod measured rod internal pressure vs. (a) measured rod void volume by manufacturer/cladding alloy, and (b) nominal beginning-of-life fill pressure of the rod by manufacturer/cladding alloy/parent assembly.



Note data for rod F35P17 are estimated.  
The abscissas values are not provided.

**Figure C-14. Measured rod internal pressure as a function of various parameters of interest (red symbols denote heat-treated sister rods).**



Note data for rod F35P17 are estimated.  
The abscissas values are not provided.

**Figure C-15. Calculated fission gas pressure as a function of various parameters of interest (red symbols denote heat-treated sister rods).**

### C-6.3 Comparisons of the Heat-Treated Sister Rod Measured Internal Pressure and Void Volume with Baseline Sister Rods

Comparisons of the measured rod internal pressure and void volume can provide some information about the effects, if any, of the heat-treatments performed on three of the sister rods. For the ZIRLO-clad rods, the heat-treated rod has a higher void volume and a higher internal pressure than the corresponding baseline rods, as shown in Figure C-13(a). However, when evaluating the measured pressure and void volume data independently of other data reported herein (e.g., transmissibility reported in Section 7.2) and considering both the measurement uncertainty and the expected variation in rod internal pressure and void volume related to operational differences, it seems unlikely that the differences between the baseline and heat-treated rod measurement results are statistically different. The M5 heat-treated rod had a higher void volume and a lower pressure than the M5 baseline rods, but the results are nearly within measurement uncertainty of each other. Thus, based only on the void volume and rod internal pressure measurements, there does not appear to be a difference between the ZIRLO- and M5-clad heat-treated rods and the baseline rods.

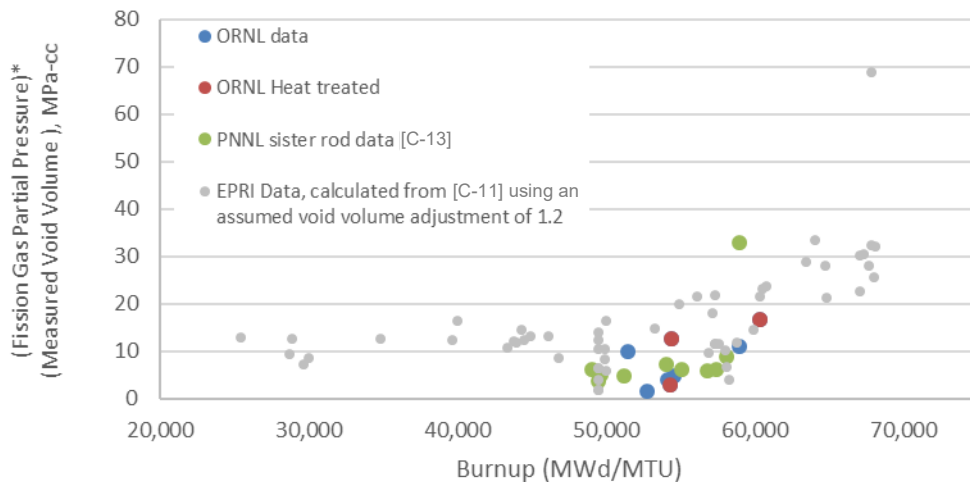
To determine if the heat treatment of the Zirc-4-clad rod made a difference in the rod internal pressure and void volume, it would be preferable to compare the results with the baseline Zirc-4 rod measured by Pacific Northwest National Laboratory (PNNL). The void volume measured by PNNL on the baseline Zirc-4 rod is ~0.7 cc lower than that measured by ORNL on the heat-treated rod, which is almost within the ORNL  $2\sigma$  volume measurement uncertainty of 0.5 cc. The rod internal pressure measured by PNNL for the baseline Zirc-4 rod is ~12% higher than that measured by ORNL for the heat-treated rod. PNNL's measurements of that rod were obtained from the bottom of the fuel rod in the pellet stack. Other than the PNNL Zirc-4-clad rod, the closest comparable baseline sister rod is an LT Zirc-4-clad rod. The void volumes of the heat-treated Zirc-4 rod and the baseline LT Zirc-4 rod are within measurement uncertainty of each other, as shown in Figure C-13(a), but the heat-treated Zirc-4 rod pressure is significantly higher than the baseline LT Zirc-4 rod. The pre-pressure of the Zirc-4 rod was 0.5 MPa higher than the LT Zirc-4 rod, but this does not account for the almost 1 MPa difference observed in the rods' end-of-life rod internal pressures. Although the Zirc-4 and LT Zirc-4 rods are very similar, differences in the rods' mechanical design could result in different end-of-life pressures and void volumes. Also, as mentioned previously, the Zirc-4 rod was a lead test rod that was operated to HBU over four cycles, while the LT Zirc-4 rod was a part of a typical batch fuel assembly operated over two cycles. Given these differences and based only on a comparison of the rod internal pressure and void volume data, it is not clear whether there was an effect related to the heat treatments on the Zirc-4-clad rod.

As a further comparison point, the product of the fission gas partial pressure and volume ( $P_fV$ ) was examined, as it tends to neutralize any lab-specific biases in the available data. The  $P_fV$  was graphed with rod average burnups, including both ORNL and PNNL [C-13] data with available EPRI data [C-11] in Figure C-16(a). It can be seen that the  $P_fV$  is relatively consistent for all the sister rods, with the exception of a single datapoint, the Zirc-4-clad rod that was punctured in the pellet stack, F35K13 [C-13]. The sister rod data are consistent with the historical database, including a change in slope occurring at ~60 GWd/MTU. To determine if there is a difference related to the heat treatments applied, Figure C-16(b) plots the available sister rod ZIRLO data, and Figure C-16(c) plots the available sister rod M5 data. It can be seen that the data for ZIRLO rods from assembly 6U3 trend very well with burnup, even given the measurements from separate labs. Data from rods from assemblies 3F9 and 3D8 are also shown, with one of the 3F9 rods being the ORNL full length rod heat treatment (FHT) rod, 3F9N05. The baseline ZIRLO rod from 3D8 appears to fit with the generally observed uptick in fission gas release shown in Figure C-16(b). It is expected that the  $P_fV$  of rods from ZIRLO assembly 3F9 would follow a trend very similar to trends for ZIRLO rods from other fuel assemblies since they are of very similar manufacture and operation. The baseline 3F9 rod  $P_fV$  is not too far from that measured for a rod having a comparable burnup. However, the FHT rod does not appear to follow the trend established by the baseline ZIRLO

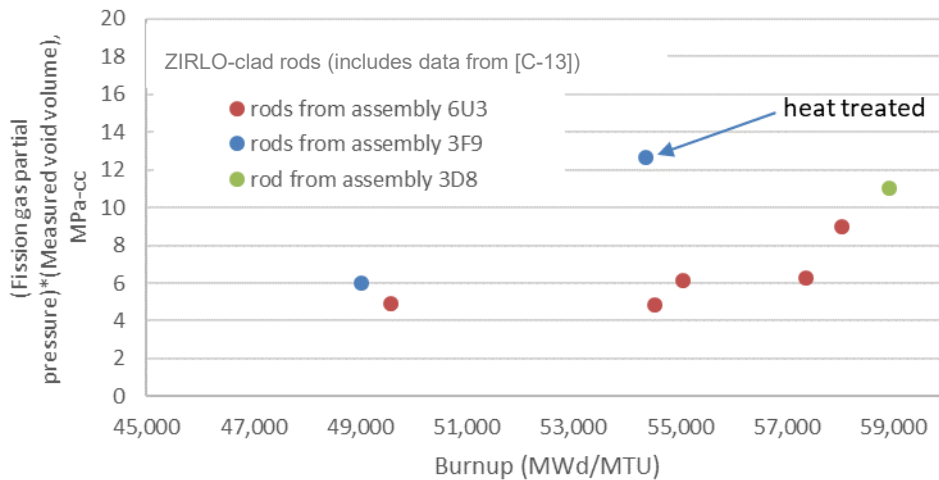


March 31, 2022

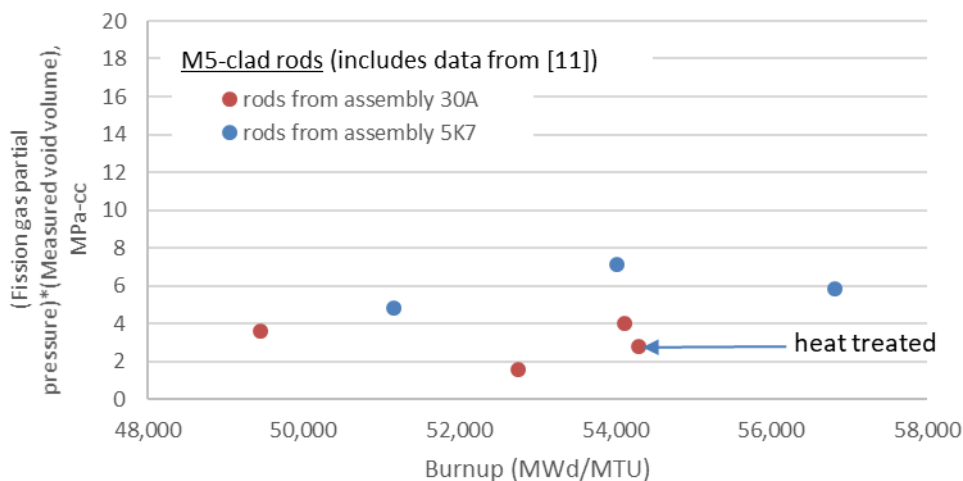
rods from assembly 6U3 and, based on Figure C-16(b), it appears that there could have been an effect on either void volume or fission gas partial pressure related to the FHT. When the same information is plotted for M5-clad rods, however, there does not appear to be an effect related to FHT, as shown in Figure C-16(c).



(a)



(b)



(c)

**Figure C-16.  $P_fV$  as a function of burnup for (a) all data to date, (b) ZIRLO-clad sister rods, and (c) M5-clad sister rods.**

## C-6.4 Comparisons of the Measured Rod Internal Pressure and Void Volume with Code Predictions

As listed in Table C-4, blind predictions of the sister rod internal pressure and void volume were made by Geelhood [C-14] using the FAST code and by Stimpson [C-15] using BISON. The two codes represent two different approaches in fuel rod modeling, with FAST providing models that are highly calibrated to a large body of empirical data and BISON operating through a more general first principles approach. This section provides a comparison of the two predictions with the measured data.

Figure C-17(a) provides a comparison of the code-predicted rod internal pressure with the measured pressure. In general, BISON tended to over-predict pressure, whereas FAST underpredicted it. FAST pressure predictions for the ZIRLO-clad 6U3 rods were within  $\pm 5\%$  of measured pressure, but other ZIRLO-clad rods from assembly 3F9 and 3D8 were within  $-25\%$  of measured pressure. All the M5-clad rods were underpredicted by FAST, with differences between  $-13$  and  $-28\%$ . The LT Zirc-4 rod pressure was also under-predicted ( $-18\%$ ) and the Zirc-4 rods were under-predicted ( $-15$  and  $-25\%$ ) by FAST. It should be noted, however, that the Zirc-4-clad sister rod F35K13 was punctured from a location in the pellet stack. The average difference between the FAST pressure prediction and the measured value is  $-14\%$ . Although the FAST code appeared to produce more accurate pressure predictions for ZIRLO-clad sister rods, the BISON predictions did not appear to have a trend related to the cladding alloy. The BISON pressure prediction difference from measured ranged from  $+10$  to  $+81\%$ , with an average difference of  $+40\%$ . Five of the BISON rod simulations did not converge [C-15].

Figure C-17(b) compares the measured void volume with the code-predicted void volume. BISON under-predicted void volume, while FAST over-predicted it most of the time. As with pressure, the FAST void volume predictions for ZIRLO-clad rods from assembly 6U3 were more accurate than predictions for other sister rods, with the average difference ranging from  $0$  to  $+14\%$ . Other than the trend noted for the 6U3 rods, there did not appear to be a cladding alloy-related trend within the FAST void volume predictions. The average difference from measured void volume for the FAST predictions was  $+20\%$ . The BISON void volume prediction average difference from measured was  $-37\%$ . The BISON void volume trends appeared relatively insensitive, producing nearly the same void volume for all rods.

The product of the rod internal pressure and void volume (PV) provides an additional metric with which to compare the measured rod data with the code predictions. The predicted rod internal pressure and void volume ( $P_p V_p$ ) are graphed with the product of the measured rod internal pressure and void volume ( $P_m V_m$ ) in Figure C-17(c). When considering PV, the FAST prediction difference from measured ranged from  $-14$  to  $+18\%$ , with an average difference of  $2\%$ . For the BISON predictions, the difference from  $P_m V_m$  ranged from  $+16\%$  to  $-26\%$ , with an average difference of  $-11\%$ .

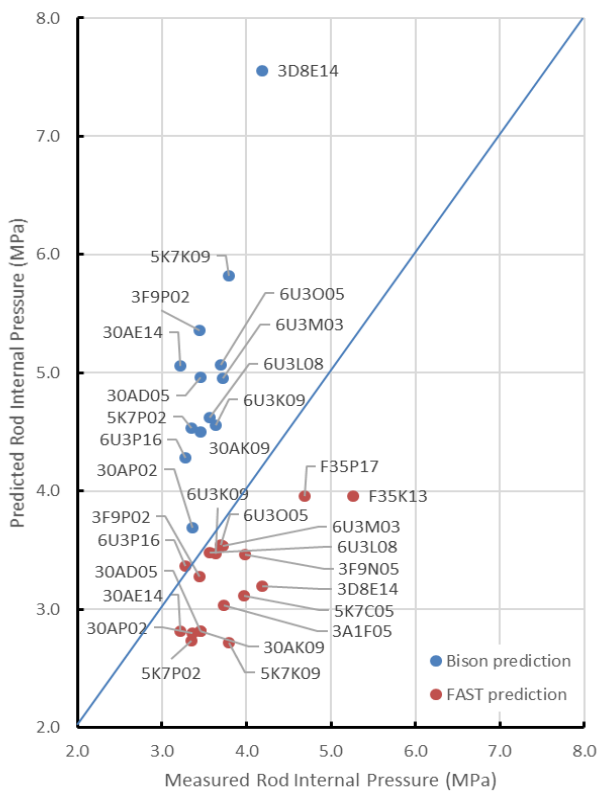
Figure C-17(d) plots the differences of predicted from measured by rod average burnup, and this plot can be used to determine if there were any trends in the differences from measured values related to rod burnup. Because the 6U3 rods were more accurately predicted by FAST, those rods are indicated on Figure C-17(d); they have a variety of rod burnups consistent with the range of burnups of the sister rods. Thus, the increased accuracy does not appear to be related to a particular range of burnup. No other obvious trends with rod burnup are visible, so it is concluded that the differences in the prediction accuracy are not related to rod burnup.

Finally, in order to provide an additional viewpoint on whether the heat treatments applied to three of the sister rods resulted in a change of the rod internal pressure or void volume, the predictions were compared graphically with ORNL's measurements (Figure C-18). It can be seen in Figure C-18 that the variations from rod to rod that were measured are consistent with variations predicted by FAST. An additional FAST calculation was completed to simulate the applied sister rod heat treatments, and there was no change to the predicted fission gas release as a result of the short time at  $400^\circ\text{C}$ . There does not appear to

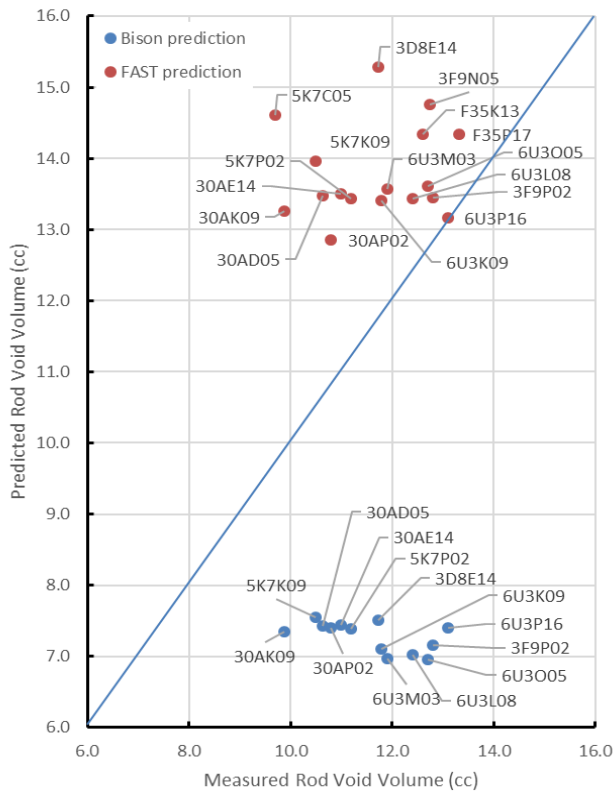
be a consistent pattern when comparing the BISON results with the measured results, and two of the BISON simulations for the rods graphed did not converge.

**Table C-4. Summary of measured and predicted rod internal pressure and void volume.**

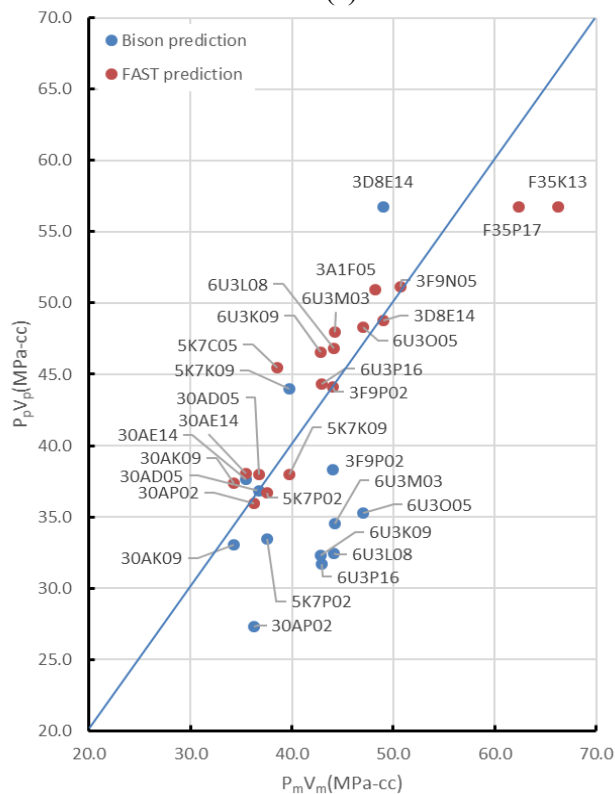
Rod ID	Cladding type	Average rod burnup	Measured rod internal pressure (MPa)	Measured void volume (cc)	FAST predicted [C-14] rod internal pressure (MPa)	Fast predicted [C-14] void volume (cc)	BISON predicted [C-15] rod internal pressure (MPa)	BISON predicted [C-15] void volume (cc)
30AD05	M5	54	3.46	10.63	2.82	13.48	4.96	7.42
30AE14	M5	54	3.22	10.99	2.82	13.50	5.06	7.44
30AK09	M5	53	3.46	9.89	2.82	13.26	4.50	7.34
30AP02 [C-13]	M5	49	3.36	10.8	2.80	12.85	3.69	7.40
5K7C05 [C-13]	M5	57	3.97	9.7	3.11	14.61	No result reported	No result reported
5K7K09 [C-13]	M5	54	3.79	10.5	2.72	13.96	5.82	7.55
5K7P02 [C-13]	M5	51	3.35	11.2	2.73	13.43	4.53	7.39
3D8E14	ZIRLO	59	4.18	11.73	3.19	15.28	7.56	7.51
3F9N05	ZIRLO	54	3.98	12.74	3.46	14.76	No result reported	No result reported
3F9P02 [C-13]	ZIRLO	49	3.44	12.8	3.28	13.45	5.36	7.15
6U3K09	ZIRLO	55	3.64	11.78	3.47	13.41	4.56	7.10
6U3L08 [C-13]	ZIRLO	55	3.56	12.4	3.48	13.44	4.62	7.02
6U3M03 [C-13]	ZIRLO	57	3.72	11.9	3.53	13.57	4.95	6.97
6U3O05 [C-13]	ZIRLO	58	3.70	12.7	3.55	13.61	5.07	6.96
6U3P16 [C-13]	ZIRLO	50	3.28	13.1	3.37	13.16	4.29	7.40
3A1F05	LT Zirc-4	51	3.73	12.94	3.04	16.77	No result reported	No result reported
F35K13 [C-13]	Zirc-4	59	5.26	12.6	3.97	14.42	No result reported	No result reported
F35P17	Zirc-4	60	4.68	13.32	3.99	14.55	No result reported	No result reported



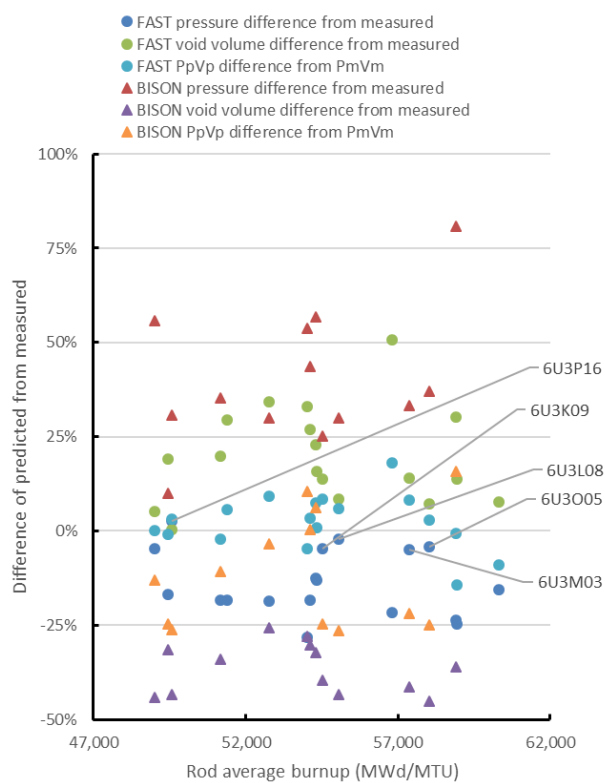
(a)



(b)



(c)



(d)

**Figure C-17. BISON- and FAST-predictions vs. measured: (a) rod internal pressure, (b) void volume, (c) product of rod internal pressure and void volume (d) difference of predicted from measured by rod average burnup.**

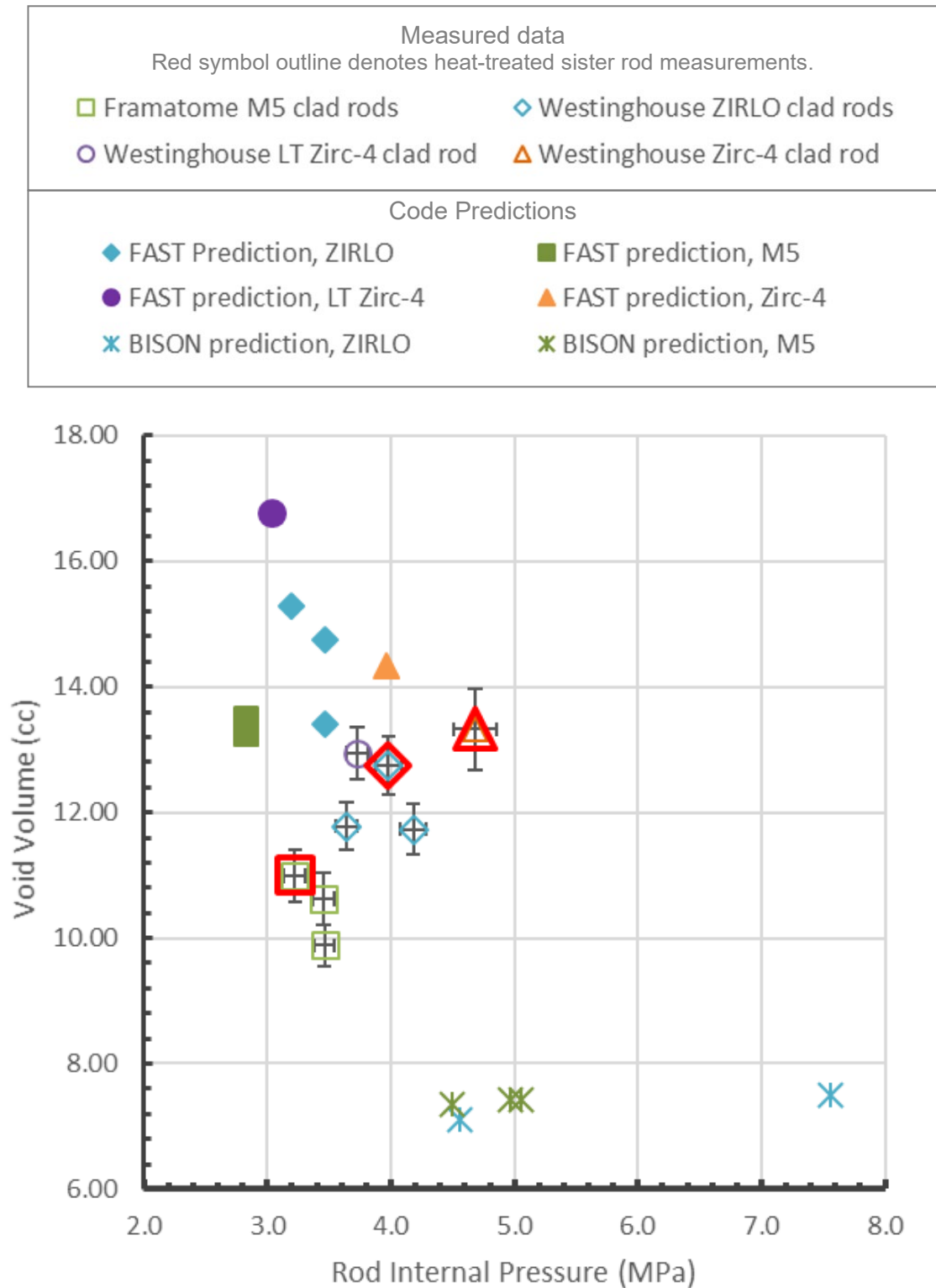


Figure C-18. Predicted rod internal pressure and void volume as compared with ORNL measurement data.

## C-7. Pellet Stack Gas Depressurization and Transmission Measurements of the Sister Rods

The measurements completed are summarized in Table C-5. The time vs. pressure recorded for the depressurization tests is shown in Figure C-19. Although some rods took longer than others to depressurize, none took longer than ~24 h to reach atmospheric pressure, demonstrating good communication along the pellet stack at room temperature. For the gas transmission tests, two sister rods were tested at three different pressures, and the recorded time vs. pressure is shown in Figure C-20. At the pressures used in the transmission tests, the time response of the system was ~30 min for one rod and ~3 h for the other. Both rods demonstrated a clear correlation between gas transmission time and applied pressure. All tests verified the ability of the argon gas to move through the pellet stack at room temperature.

**Table C-5. Results of depressurization and transmission tests.**

Rod	Applied pressure differential (MPa)	Muskat-Poiseuille permeability and regression model coefficient of determination	
		K (m <sup>2</sup> )	R <sup>2</sup>
3A1F05	0.10	8.40E-14	0.999
	1.41	8.32E-14	0.999
	2.17	8.32E-14	1.000
	2.89	8.23E-14	1.000
	<i>Average</i>	<i>8.32E-14</i>	
F35P17	0.10	9.96E-14	0.999
3F9N05	0.10	7.30E-14	0.999
3D8E14	0.10	4.08E-14	0.998
6U3K09	0.10	1.99E-14	1.000
	1.55	1.62E-14	0.994
	2.82	2.05E-14	1.000
	<i>Average</i>	<i>1.89E-14</i>	
30AK09	0.10	1.04E-14	0.999
	1.41	1.02E-14	0.999
	2.17	1.05E-14	1.000
	2.89	1.11E-14	1.000
	<i>Average</i>	<i>1.06E-14</i>	
30AD05	0.10	1.15E-14	1.000
30AE14	0.10	2.40E-14	1.000
<i>Average of all</i>		<i>4.25E-14</i>	

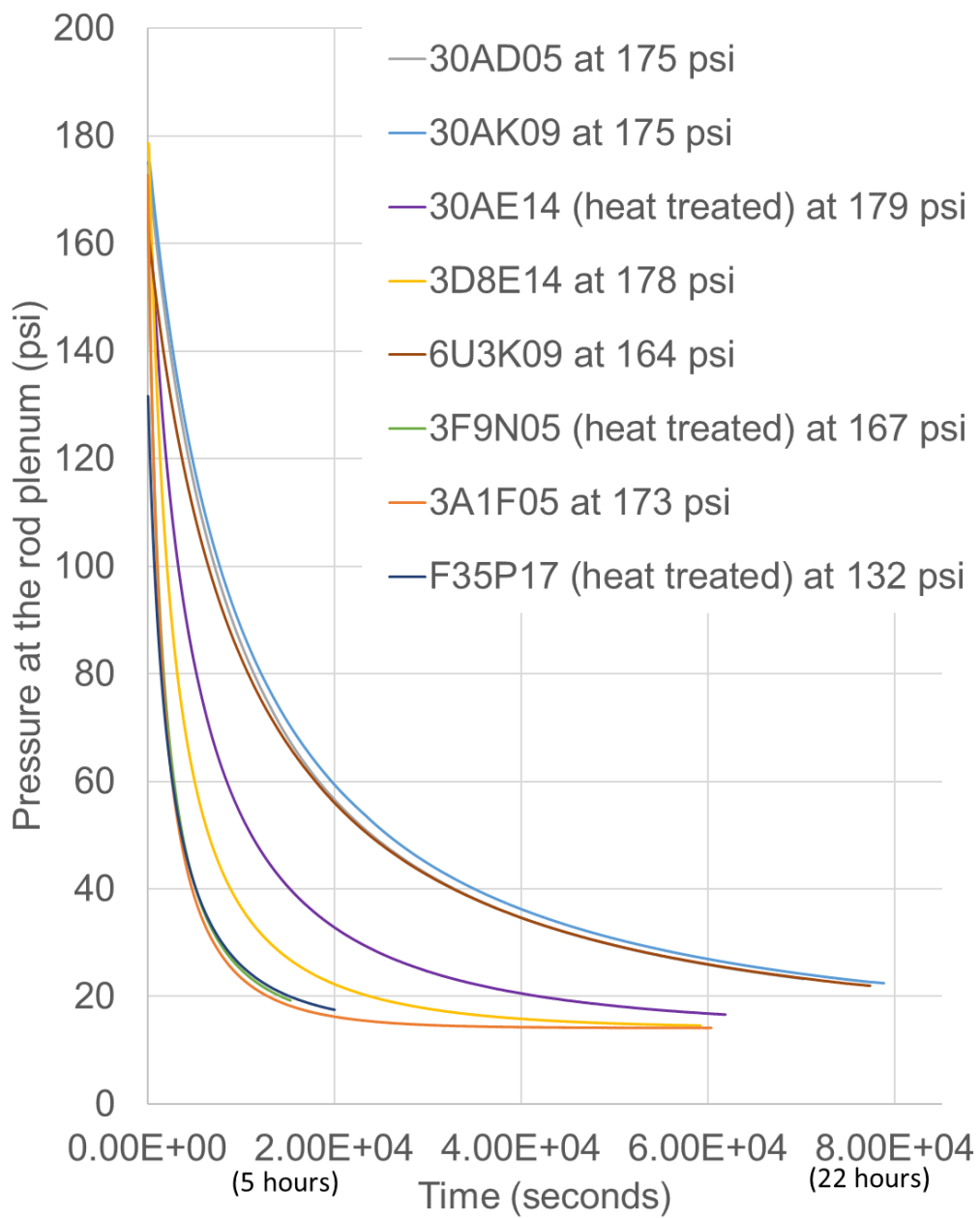


Figure C-19. Results of the depressurization tests on 8 sister rods (3 rods were heat-treated).

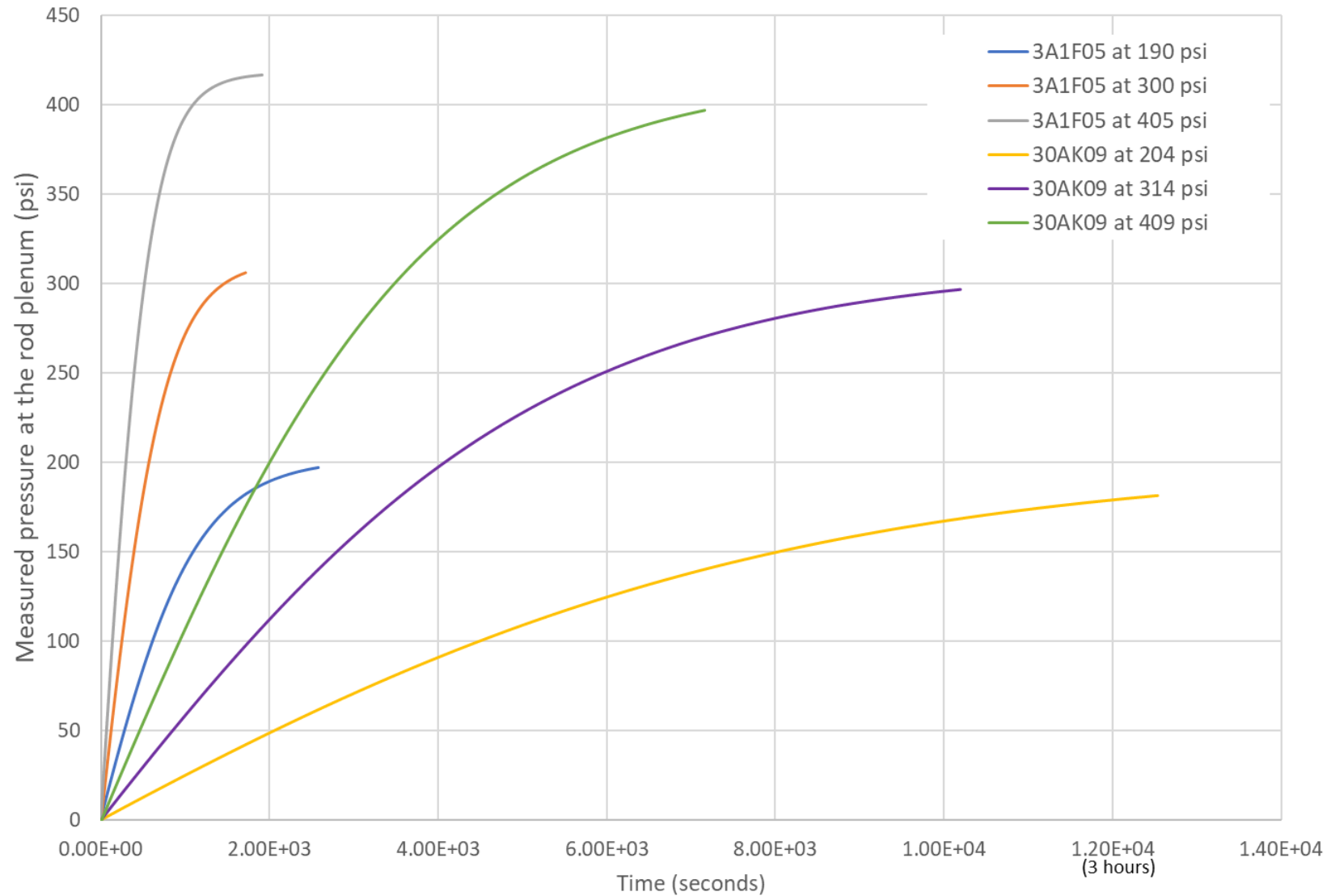


Figure C-20. Results of gas transmission tests on 2 sister rods (3 different pressures on each rod).



Figure C-21 illustrates the predicted time vs. pressure using the Muskat-Poiseuille correlation. The Muskat-Poiseuille prediction fits well, indicating that the assumption of compressible gas flow is necessary and appropriate. For comparison purposes, the data were also fit using Darcy's Law, which assumes incompressible flow, and is plotted in Figure C-21. As expected, the incompressible flow model predictions do not fit the data well.

The permeability of the pellet stack varied over less than an order of magnitude for this set of rods, which is modest and may indicate some common feature about HBU fuel. The average permeability for the HBU  $17 \times 17$  PWR fuel rods is  $4.25 \times 10^{-14} \text{ m}^2$  using the Muskat-Poiseuille model. These results are about 20% of that measured by Rondinella [C-9] and correlated using Darcy's Law at  $2 \times 10^{-13} \text{ m}^2$ . Comparison of the average low-pressure Darcy porosity measured for the sister rods,  $1.6 \times 10^{-13} \text{ m}^2$ , with Rondinella's results shows that the data are comparable if the same level of precision is applied. Rods 3A1F05 (LT Zirc-4) and F35P17 (heat-treated Zirc-4) have the largest permeability values, with the variance likely due to the wide variety of clads, pellets designs, and operating histories. Note that the higher the evaluated permeability, the more easily the fission gases can move through the pellet stack.

Regarding the three rods on which the gas transmission test was repeated at varying starting pressures, it appears that the permeability maintains a relatively constant value with pressure variation, as shown in Figure C-22. For the tests results reported herein, the time constants ( $l/\eta K$ ) are exaggerated because of the rather large tare volume associated with the hardware required for hot cell testing. Without the tare volume, the time constants are expected to be approximately  $\frac{1}{3}$  of that shown in the graphs. Although argon was used instead of helium, xenon, and krypton, the general results are not expected to be significantly influenced by the gas mixture if the proper viscosity is used.

To examine whether differences in rod operation result in different permeability, the evaluated Muskat-Poiseuille permeability was plotted against available operational parameters, including rod average burnup, high duty core index (HDCI) [C-16], and predicted assembly average middle-of-cycle fuel temperature, as shown in Figure C-23. Unfortunately, while the average rod burnup for rod F35P17 is known [C-17], the rod's operating temperatures are not available at this time, so the values for HDCI and temperature shown are estimated. It appears that there is no close correlation with the rod's average burnup. Maximum rod HDCI appears to be somewhat correlated, as does the assembly's average fuel temperature. However, it is not clear if this is a global trend or if it is only related to this particular set of HBU fuel rods. The permeability does appear to be closely related to the rod manufacturer, as illustrated when the Muskat-Poiseuille permeability is plotted by cladding type (Figure C-23d). Based on the results shown in Figure C-23, it seems that the pellet manufacturing process and operating temperature determine the permeability of the pellet stack. Furthermore, the three rods that were heat-treated to simulate a dry storage vacuum drying environment (to the regulatory guidance temperature limit) are indicated in Figure C-23. Although Figure C-23 a, b and c do not provide conclusive evidence that the heat treatment affected the permeability, Figure C-23d does strongly indicate that an offset in the permeability could have resulted from the heat treatment. However, there are not enough data available to reach the conclusion that a statistical difference exists.

A natural extension of this work is to conduct the same tests at the fuel rod storage and transportation temperatures using a similar apparatus. Also, it would be prudent to measure gas transmissibility on rods that have been in dry storage for  $\sim 10$  years to determine if the flow paths have become restricted.

All tests were completed at room temperature, and the influence of temperature on transmissibility has not been explored. Some change in permeability due to thermal expansion effects is expected, and repeating the tests at a higher temperature that is representative of transportation/storage is recommended.

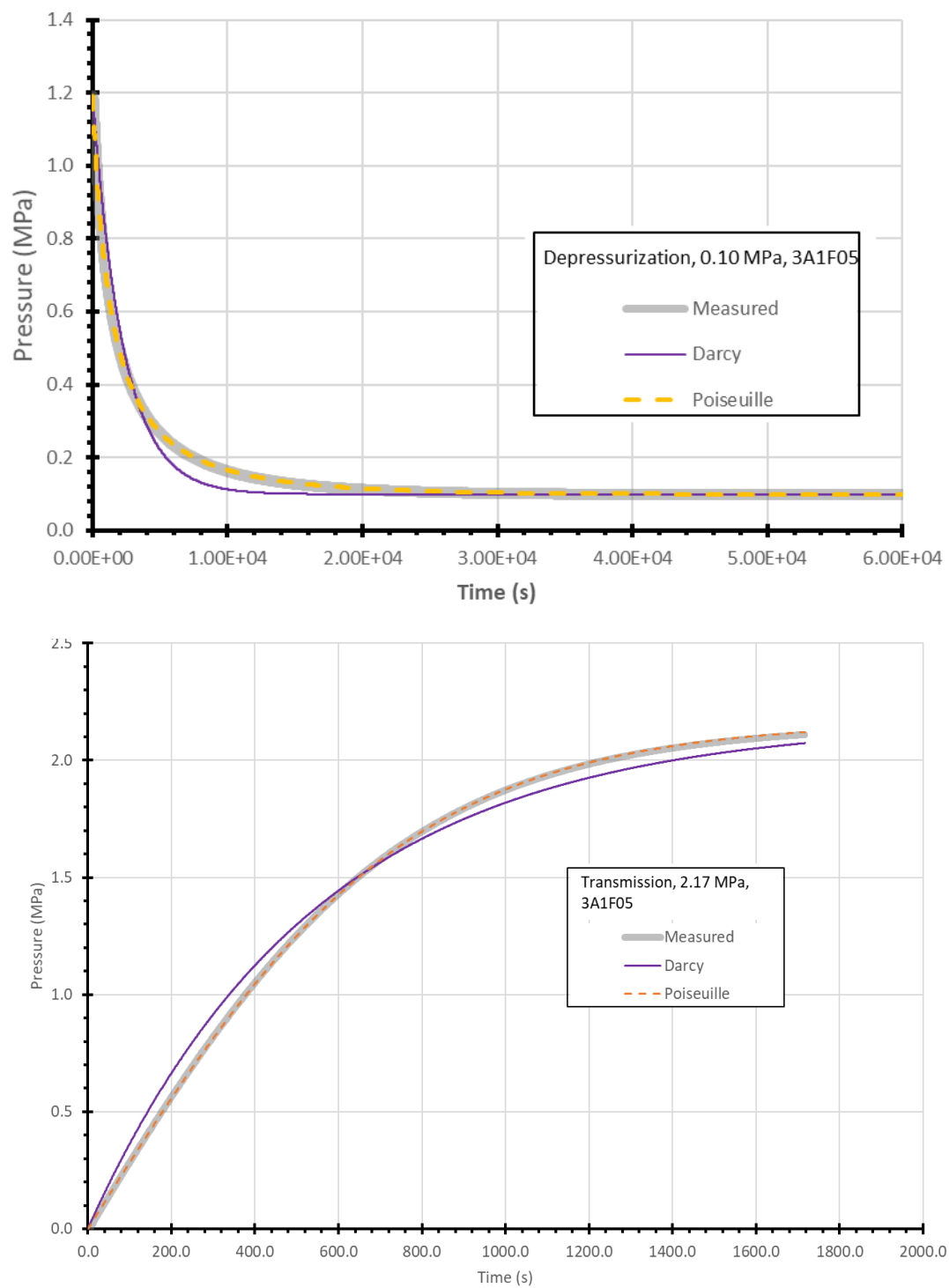


**Figure C-21. Pressure vs. time predictions using the Muskat-Poiseuille model for compressible gas flow and Darcy's law for incompressible flow for sister rod 3A1F05: depressurization (top) and gas transmission (bottom) test results.**

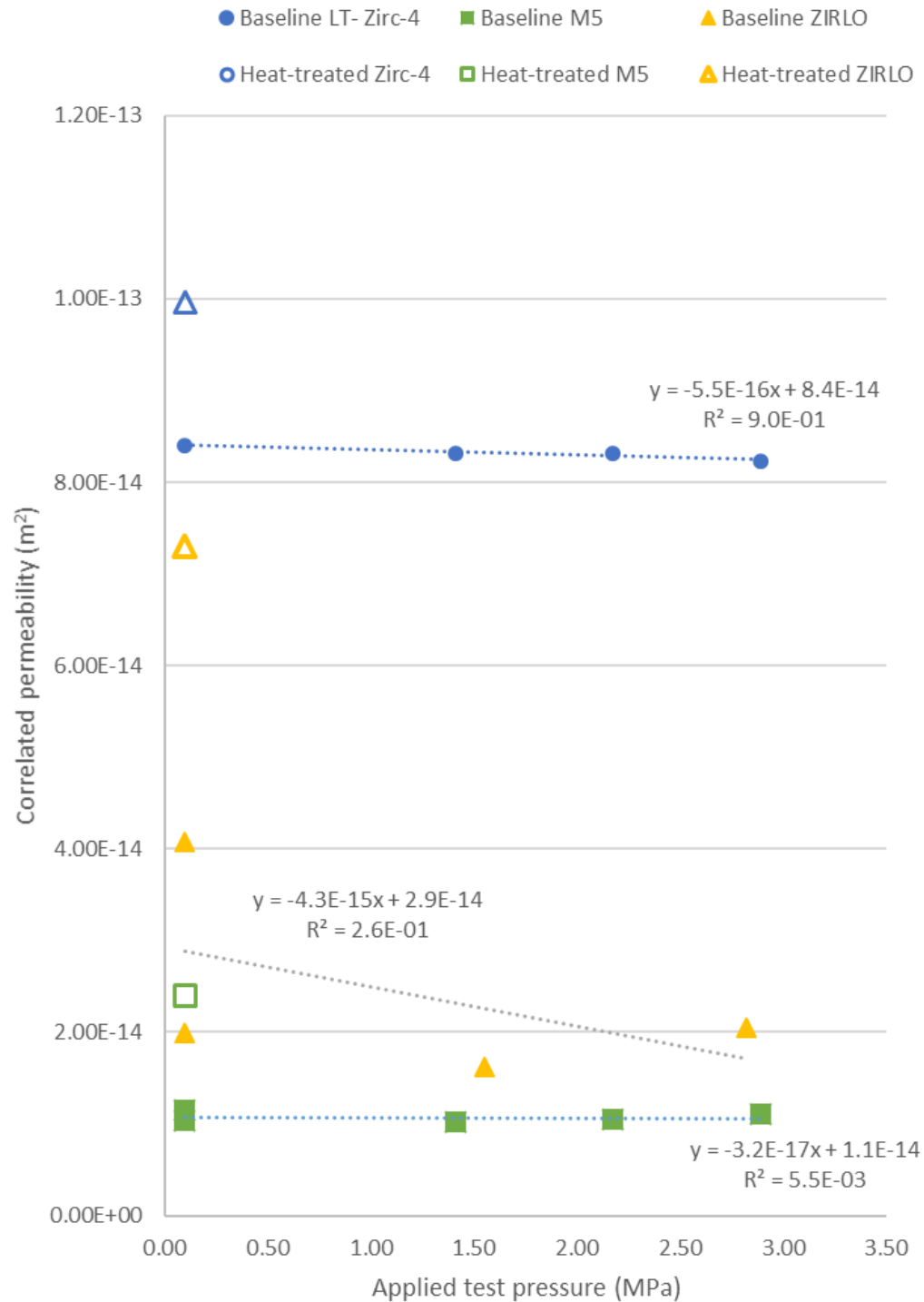
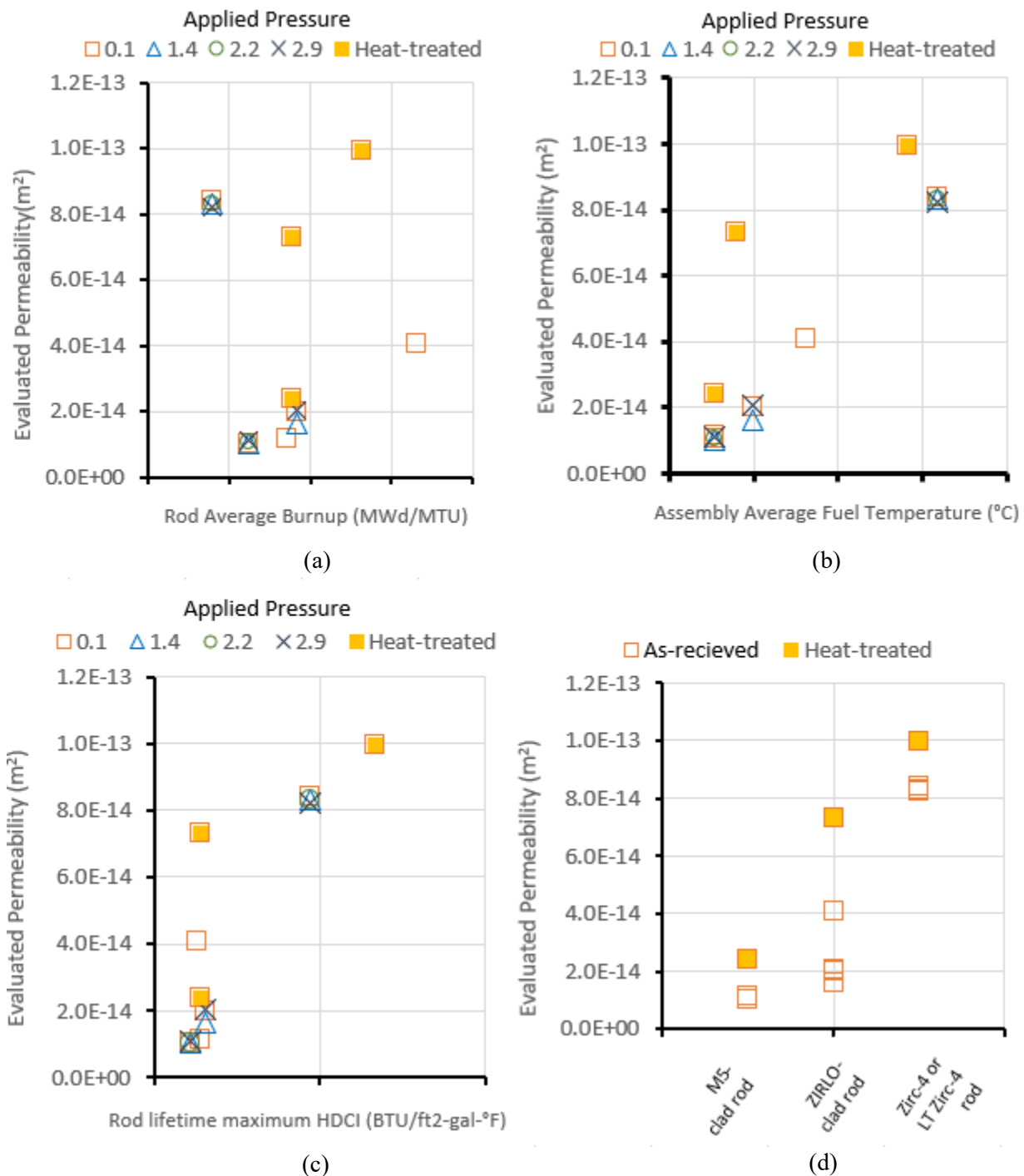


**Figure C-22. Evaluated Muskat-Poiseuille permeability for baseline rods subjected to transmission tests at various driving pressures by cladding type and heat-treatment.**



Note the abscissas values are not provided.

**Figure C-23. Evaluated Muskat-Poiseuille permeability as a function of (a) rod average burnup, (b) assembly average fuel temperature during operation, (c) estimated rod HDCI, and (d) rod cladding type (also reflective of the rod manufacturer and vintage).**

## C-8. Fission Gas Release Calculations

Table C-3 in Section C-6.1 provides the rod pre-pressurization, measured post-irradiated rod internal pressure, void volume, and rod average burnup for the phase 1 sister rods that were punctured. A small sample of the gas within the rod was analyzed to determine the mole distribution of helium, krypton, and xenon. The majority of the helium is from pre-pressurization during the fabrication process. The analysis of the mole distribution of helium, krypton and xenon was reported in Appendix D, Table D-3.

The following assumptions are applied:

- The gas within the fuel rod is assumed to be an ideal gas.
- No additional fission gas was released after discharge from the reactor.
- All the major isotopes of He, Kr and Xe are stable except for  $^{85}\text{Kr}$ , which has a half-life of 10.776 yr. Because  $^{85}\text{Kr}$  is only ~6% of the total Kr inventory, and Kr contributes only ~10% to the rod internal pressure, the small change in moles Kr due to decay is considered insignificant and will be ignored
- He generated from fission product decay after reactor discharge is ignored

Three gaseous elements are considered in this calculation: He, Kr, and Xe. The calculation of percent fission gas release only considers Kr and Xe, which are a direct result of the fission process. Helium is considered separately because its source is mostly from decay processes rather than the fission process.

The fission gas release fraction in terms of moles is given by

$$f_{\text{fission gas release}} = \frac{n_{\text{Kr-gas}} + n_{\text{Xe-gas}}}{n_{\text{Kr-inventory}} + n_{\text{Xe-inventory}}}, \quad (\text{C-86})$$

where *inventory* refers to the Kr and Xe available to be released (i.e., the moles of Kr and Xe created from the fission process).

The number of moles released can be calculated assuming the fission gas is an ideal gas. Therefore, the total number of moles of gas in a fuel rod is

$$n_T = \frac{PV}{RT}, \quad (\text{C-87})$$

where  $n_T = n_{\text{He}} + n_{\text{Kr}} + n_{\text{Xe}}$ .

Thus, the total number of moles of gas can be calculated based on the measured pressure and void volume from the gas puncture tests (see Table C-3).

The number of moles of each gas element is  $n_T f_g$ , where  $f_g$  is the mole fraction of that element within the fuel rod gas [C-2, Table D-3]. Thus,

$$\begin{aligned} n_{\text{He}} &= n_T f_{\text{He}}, \\ n_{\text{Kr}} &= n_T f_{\text{Kr}}, \text{ and} \\ n_{\text{Xe}} &= n_T f_{\text{Xe}}. \end{aligned} \quad (\text{C-88})$$

The number of moles of He in the gas includes both the He from pre-pressurization and that released during irradiation. The number of moles of Kr and Xe are considered to be fission gas released during irradiation.

The isotopic mass distribution for Kr and Xe was calculated by Cumberland [C-18].

The total moles of Kr and Xe in the inventory can be calculated by summing up the moles of the individual isotopes. Given that the output of the nuclear calculations is a distribution of grams of isotope [C-4], the total moles of Kr and Xe are

$$n_{Kr-inventory} = \sum_i \frac{m_{Kr[i]-inventory}}{M_{wKr[i]}} \text{ and} \quad (C-89)$$

$$n_{Xe-inventory} = \sum_i \frac{m_{Xe[i]-inventory}}{M_{wXe[i]}}$$

where  $m_{X[i]-inventory}$  is the mass and  $M_{wX[i]}$  is the molecular weight of isotope  $i$  of Kr and Xe.

Table C-6 provides the calculated moles of Kr and Xe after discharge per the method described in Section C-8.2. Table C-7 documents the calculated percent fission gas released using Eq. [C-86], where the moles of Kr and Xe in the inventory are calculated per the method described in Section C-8.2. The percent fission gas released was calculated for the sister rods that were gas punctured at ORNL. The percent fission gas released for all the rods is in the range of 1.5 to 3.5%.

Figure C-24 compares the sister rod data to available open literature data used to support the FAST thermal-mechanical fuel performance code [C-19]. Overall, the sister rod data has low fission gas release compared to the open literature data, but the open data mainly includes European-operated rods. The sister rod data are similar to data from rod IFA-597.3 that had a measured fission gas release of 2.5–3.3% after operating in Ringhals for 12 years to an exposure 52 GWd/MTU (rod average)[C-20]. A comparison of the calculated percent fission gas release to the predicted fission gas release by FAST [C-14], which includes the effect of power history, is favorable.

**Table C-6. Calculated moles of Kr and Xe in gas after discharge.**

Rod ID	Rod Internal Pressure after Discharge (MPa)	Void Volume after Discharge (cm <sup>3</sup> )	Moles of gas after Discharge (mole)	Fraction of Kr in gas	Fraction of Xe in gas	Xe/Kr
30AK09	3.46	9.89	0.0138	0.016	0.153	9.563
30AD05	3.46	10.63	0.0148	0.014	0.141	10.071
30AE14	3.22	10.99	0.0143	0.015	0.141	9.400
3D8E14	4.18	11.73	0.0198	0.024	0.224	9.333
3F9N05	3.98	12.74	0.0205	0.023	0.201	8.739
6U3K09	3.64	11.78	0.0173	0.011	0.105	9.545
3A1F05	3.73	12.94	0.0195	0.020	0.185	9.250

**Table C-7. Calculated percent fission gas released.**

Rod ID	Moles of Kr and Xe gas after discharge (mole)	Moles of Kr and Xe in the inventory after discharge (mole)	Percent fission gas released	FAST predicted percent fission gas release [C-14]
30AK09	0.0023	0.1225	1.9%	1.78%
30AD05	0.0023	0.1258	1.8%	1.92%
30AE14	0.0022	0.1262	1.8%	1.95%
3D8E14	0.0049	0.1374	3.6%	2.46%
3F9N05	0.0046	0.1263	3.6%	3.38%
6U3K09	0.0020	0.1269	1.6%	1.99%
3A1F05	0.0040	0.1201	3.3%	3.44%

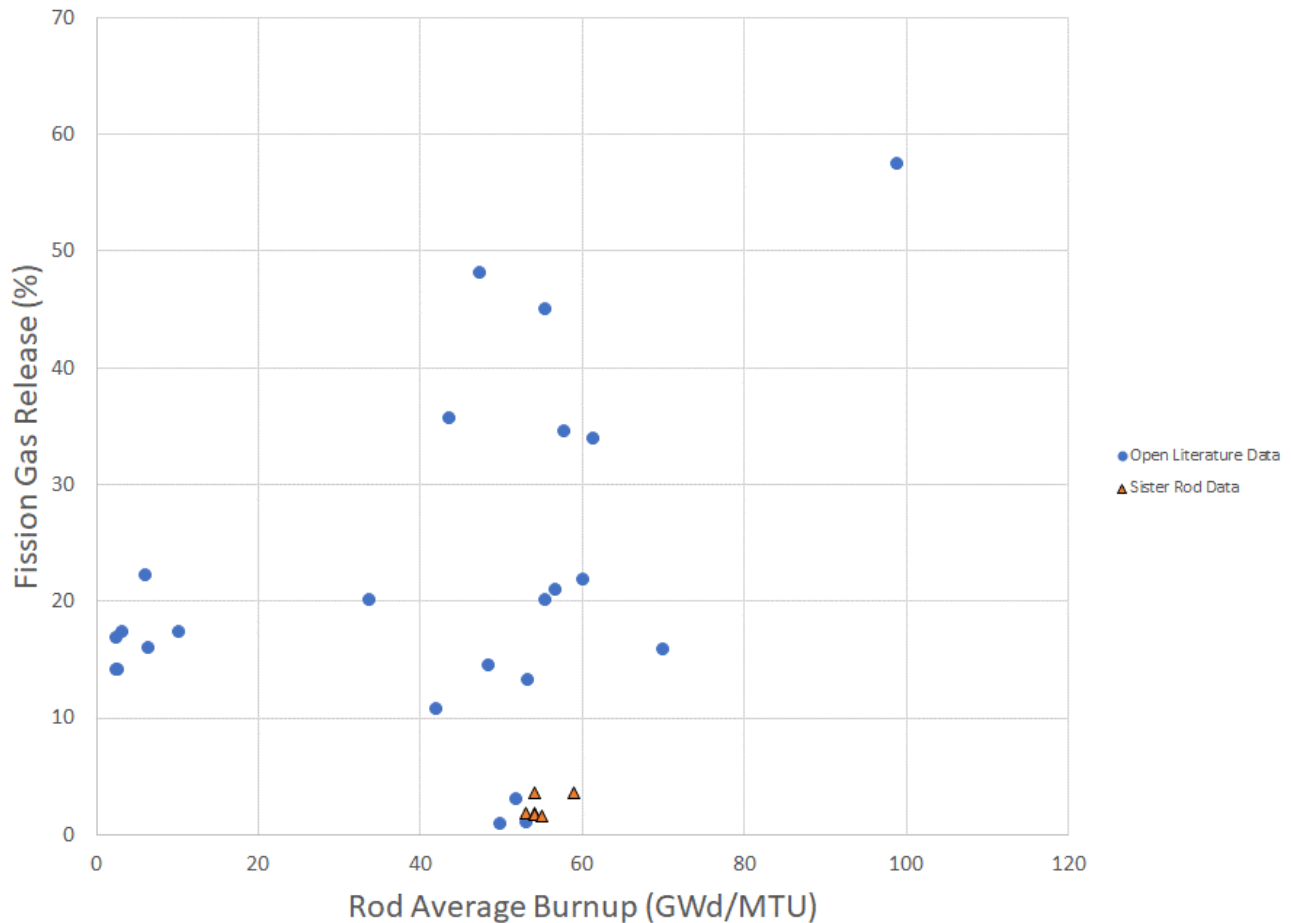


**Figure C-24. The calculated percent fission gas release of the sister rods compared to open literature data [C-19] and [C-20].**

## REFERENCES

- [C-1] *High Burnup Dry Storage Cask Research and Development Project: Final Test Plan*, contract no. DE-NE-0000593, Electric Power Research Institute, Palo Alto, California (2014).
- [C-2] Saltzstein, S. et al., *Visualization of the High Burnup Spent Fuel Rod Phase I Test Plan*, SAND2018-8042-O (2018).
- [C-3] Montgomery, R. A. et al., *Post-Irradiation Examination Plan for High Burnup Demonstration Project Sister Rods*, SFWF-SFWST-2017-000090 ORNL/SR-2016/708, Oak Ridge National Laboratory (2016).
- [C-4] Bandyopadhyay, G. T., A. Roberts, “Crack Healing and Strength Recovery in  $\text{UO}_2$ ,” *J. Am. Ceram. Soc.* **59**, 415 (2005), 419. 10.1111/j.1151-2916.1976.tb09508.x.
- [C-5] Cuta, J. M., S. R. Suffield, J. A. Fort, and H. E. Adkins, *Thermal Performance Sensitivity Studies in Support of Material Modeling for Extended Storage of Used Nuclear Fuel*, Pacific Northwest National Laboratory, FCRD-UFD-2013-000257 PNNL-22646 (2013).
- [C-6] Desgranges, L., M. Faure, and A. Thouroude, “A New Apparatus for Determination of the Void volume of a Fuel Rod Using the Double Expansion Method,” *Nucl. Technol.* **149**, 14–21 (2005).
- [C-7] Dagbjartsson, S. J. et al., *Axial Gas Flow in Irradiated PWR Fuel Rods*, TREE-NUREG-1158 (1977).
- [C-8] Calogivic, V., “Gas Permeability Measurement of Porous Materials (Concrete) by Time-Variable Pressure Difference Method,” *Cement and Concrete Research* **25**. No. 5.1054–1062 (1995).
- [C-9] Rondinella, V. V. et al., “Measurement of Gas Permeability Along the Axis of a Spent Fuel Rod,” Top Fuel 2015, Zurich, Switzerland (2015).
- [C-10] Muskat, M., “The Flow of Compressible Fluids Through Porous Media and Some Problems in Heat Conduction,” *Physics* **5**, 71–94, (1934), doi: 10.1063/1.1745233.
- [C-11] *End-of-Life Rod Internal Pressures in Spent Pressurized Water Reactor Fuel*, 3002001949, Electric Power Research Institute, Palo Alto, California (2013).
- [C-12] Pan, G., et al. “Performance Characteristics of High Burnup ZIRLO Cladding Fuel Rods,” Proceedings of TopFuel/Global Fuel Performance Meeting, Seattle, WA (2019).
- [C-13] R.W. Shimskey et al. *PNNL Phase I Update on Sister Rod Destructive Examination Results*, SFD-SFWST-M2SF-19PN010201037, Pacific Northwest National Laboratory, September 2019 [pending release].
- [C-14] K. Geelhood, *Sister Rod Thermomechanical Modeling with FAST*, PNNL-28224 [pending release].
- [C-15] S. Stimpson, *Sister Rod Predictions of End-of-Life Rod Internal Pressure and Void Volume*,” ORNL/SPR-2019/1173 M4SF-19OR0102010210, Oak Ridge National Laboratory (2019).
- [C-16] *PWR Axial Offset Anomaly (AOA) Guidelines*, Revision 1, EPRI, Palo Alto, CA, 1008102 (2004).
- [C-17] M.G. Balfour et al. *Corrosion of Zircaloy-Clad Fuel Rods in High-Temperature PWRs” Measurement of Waterside Corrosion in North Anna Unit 1, TR-100408 Tier 2*, Research



Project 2757-1, Westinghouse Electric Corporation for Electric Power Research Institute, March 1992.

- [C-18] R. Cumberland, *High Burnup Storage Demonstration Sister Rod Depletion Calculations*, Excel file Inventory\_03042019.xlsx, ORNL/SRP-2020/1439 [pending release].
- [C-19] K. Geelhood et al., *Fast-1.0.1: Integral Assessment*, PNNL-31161, April 2021.
- [C-20] Nuclear Energy Agency, *International Performance Experiments (IFPE) database*, IFA-597.3, rod 8, <https://www.oecd-nea.org/tools/abstract/detail/nea-1685>.